Electrostrictive and Piezoelectric Effects in Relaxor Ferroelectrics: Historical Background

Kenji Uchino, *Life Fellow, IEEE*

***Abstract*— Electrostrictive effects in complex-perovskite "relaxor" ferroelectrics (FEs) exhibit superior performance in comparison with the simple-perovskite normal FEs, such as giant electrostriction in its paraelectric phase and high electromechanical coupling in its FE phase. As one of the discoverers, the author will deliver the historical background of these epoch-making phenomena and the development strategy of how we considered performance improvement. Though both discoveries were actually originated from a sort of "serendipity" (lucky & accidental occurrence!), some of the key factors have been embedded in the research base: 1) interrelation between complex perovskite structure and ferroelectricity; 2) anharmonicity in relaxor FEs; and 3) microdomain contribution in relaxor FEs. In the last part of this article, the author introduces a bit different "mesoscopic" approach, "fractal analysis of microdomain configuration" in conjunction with the "domain engineering" concept, to distinguish the electromechanical coupling among the normal and relaxor FEs for remaining the future research seeds.**

***Index Terms*— Critical exponent, dielectric relaxation, diffuse phase transition, disordered perovskite, domain engineering, fractal dimension, giant electrostriction, lead–magnesium–niobate (PMN), lead–zinc–niobate (PZN), relaxor ferroelectrics (FEs).**

I. Introduction: Background of Electrostrictiive Effect

CROSS *et al.* [1] reported giant electrostriction higher than 0.1% of the strain observed in lead–magnesium–niobate-based ceramics (PMN-PT) in the late 1970s, which has immediately accelerated the ceramic actuator applications [1]–[3]. In parallel, Kuwata *et al.* [4], [5] also discovered a superior electromechanical coupling effect with k_{33}* higher than 95% in lead–zinc–niobate-based single crystals (PZN-PT). These epoch-making discoveries in the last 20th century, both of which were originated from a sort of "serendipity," lead to further intensive investigations in the present 21st century from both viewpoints of theoretical modeling and practical transducer applications.

Manuscript received 22 February 2022; accepted 2 April 2022. Date of publication 7 April 2022; date of current version 2 November 2022. This work was supported by the U.S. Office of Naval Research Code 332 under Grant N00014-91-J-4145, Grant 92-J-1510, Grant 96-1-1173, Grant 99-1-0754, Grant 08-1-0912, Grant 12-1-1044, Grant 17-1-2088, and Grant 20-1-2309.

The author, retired, was with the Department of Electrical Engineering, The Pennsylvania State University, State College, PA 16801 USA (e-mail: kxu1@psu.edu).

Digital Object Identifier 10.1109/TUFFC.2022.3165002

This article delivers the historical background of these discoveries, aiming at providing key factors for understanding why the relaxor/complex perovskites exhibit superior electrostrictive/electromechanical coupling and for developing new materials for actuators and transducers from the author's personal strategies. These factors may include: 1) interrelation between complex perovskite structure and ferroelectricity; 2) anharmonicity in relaxor ferroelectrics (FEs); and 3) microdomain contribution in relaxor FEs. After this introduction (see Section I), the following sections are composed of electrostriction phenomenology, including both FEs and antiferroelectrics (AFEs) (see Section II), complex perovskites for discussing the FE properties in terms of ionic ordering and the empirical "QC constant rule" (see Section III), the microscopic origin of electrostriction (see Section IV), characterization methods of electrostriction, and obtained results for both normal and relaxor FEs, and then, the key sections (see Section V), anharmonicity of lattice vibration in relaxor FEs for discussing the smaller electrostrictive coefficient and larger Curie–Weiss constant in relaxors, in comparison with normal types (see Section VI), critical exponent in relaxor FEs, which indicates microdomain–microdomain interaction in a crystal (see Section VII), leading to fractal analysis of microdomain configuration (see Section VIII). This section may be a bit different mesoscopic approach to distinguish the electromechanical coupling among the normal and relaxor FEs in terms of nanodomain, microdomain, and macrodomain configurations, which provides direct insight into the domain configurations for the piezoelectric performance improvement in the domain engineering (see Section IX). This is not a comprehensive review paper for covering extensive up-to-date research. Regarding various actuator/transducer applications of these materials, refer to other references, such as a textbook [92].

A. Discovery of Giant Electrostriction

The "Space Shuttle" project planned to install a deformable mirror in the middle of the 1970s in order to control the optical pathlengths over several wavelengths (~1 μm) for obtaining much better resolution in astronomical pictures (i.e., "Hubble Telescope"). Precise "displacement transducers" (initially used terminology) were required for this application. Because the conventional piezoelectric PZT ($Pb(Zr,Ti)O_3$) ceramics were plagued by hysteresis and zero-point drift

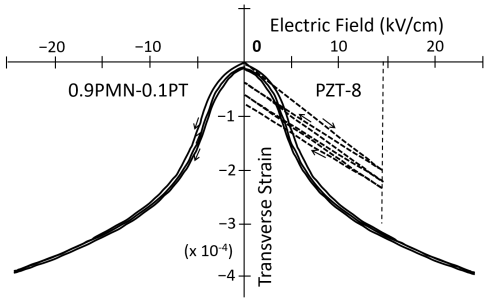

Fig. 1. Transverse strain curves in ceramic specimens of 0.9PMN-0.1PT and typical hard PZT 8 piezoceramic under varying electric fields [1].

of strain under large electric fields (a serious problem for an optical positioner), gigantic electrostriction invented by Cross *et al.* [1] with the strain level higher than 0.1% with negligible hysteresis during rising and falling electric field in a composition $0.9Pb(Mg_{1/3}N_{2/3})O_3$-$0.1PbTiO_3$ [0.9PMN-0.1PT] was eagerly desired (see Fig. 1). The reader knows that every phenomenon has primary and secondary effects, which are recognized usually as linear and quadratic phenomena, respectively. In actuator materials, these correspond to the "piezoelectric" and "electrostrictive" effects. Though many people believed that the secondary effect would be minor and could not provide a contribution larger than the primary effect, the enormous electrostriction was actually discovered in relaxor FE PMN-PT solid solutions in their paraelectric phase, larger than the PZT piezostriction, as demonstrated in Fig. 1. The "serendipity" here means that we just started to measure them merely because we had plenty of these complex perovskite ceramic specimens in our lab. Though we spent more than three years on other kinds of specimens, including PZT-based ceramics, we found that this first composition exhibited accidentally the highest electrostriction value under an electric field of 1 kV/mm, which was a safety limit in the "Industrial Standard" then.

This discovery, in conjunction with the multilayer (ML) actuator invention by Uchino *et al.* [3], accelerated the development of "piezoelectric/electrostrictive actuators" after the 1980s [6]. The "Hubble" telescope proposed by the Jet Propulsion Laboratory, NASA, by using six ML PMN electrostrictive actuators to control the phase of the incident light wave was successfully launched on the Space Shuttle in 1993 [7].

B. High Electromechanical Coupling Relaxor Single Crystals

Uchino's group at the Tokyo Institute of Technology was interested in making single crystals of PZT in the 1970s in order to clarify the crystal orientation dependence of piezoelectricity. However, it was difficult for them to prepare large single crystals with the "morphotropic phase boundary (MPB)" composition (52/48). Thus, the $Pb(Zn_{1/3}Nb_{2/3})O_3$-$PbTiO_3$(PZN-PT) solid solution system was focused instead because it could easily be prepared in large single-crystal forms with a phase diagram similar to the PZT system. See the MPB between the rhombohedral

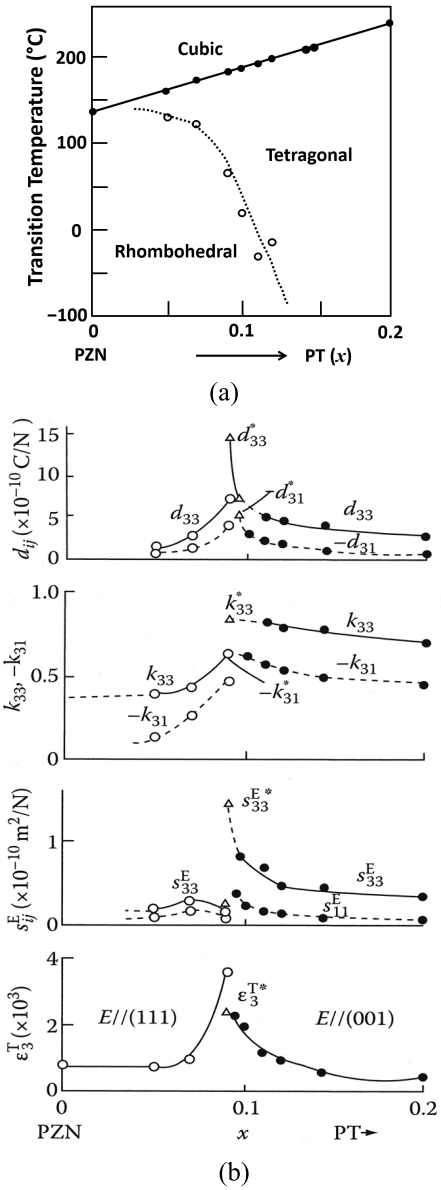

Fig. 2. (a) Phase diagram for the $Pb(Zn_{1/3}Nb_{2/3})O_3$–$PbTiO_3$ solid solution system. (b) Changes of electromechanical coupling factors with PT in the $Pb(Zn_{1/3}Nb_{2/3})O_3$–$PbTiO_3$ system.

and tetragonal phases in Fig. 2(a) [4]. Fig. 2(b) shows the dependence of electromechanical coupling parameters on the PT amount in the $(1-x)$PZN-xPT system, reported by Kuwata *et al.* [5] in 1982. Note that the MPB composition, 0.91PZN-0.09PT, exhibited the maxima for all parameters, in particular, the highest values in electromechanical coupling factor $k_{33}{}^*$ and the piezoelectric constant $d_{33}{}^*$ reached 95% and 1600 pC/N, respectively, when the poling direction was along the perovskite ⟨100⟩ direction, 57° canted from the spontaneous polarization (P_S) direction (perovskite ⟨111⟩ direction), not along the P_S direction. Superscript * was used because the poling direction was not along the spontaneous direction (i.e., different from the definition of d_{33}). When a Ph.D. student, J. Kuwata, reported to the author first, even I could not believe these large numbers. Thus, we worked together

to reexamine the experiments. When I saw the antiresonance frequency almost twice the resonance frequency, I needed to believe this incredibly high k value in 1980. The author still remembers that the first submission of our manuscript was rejected because the referee could not "believe this large value." The maximum k_{33} in the 1970s was about 72% in the PZT-based ceramics. This article was published after a year-long communication by sharing the raw admittance curves and so on via "sea mail" then. However, our original discovery was not believed or not required for applications until the middle of the 1990s. A sort of "best-citation note" arrived at us 17 years after the discovery. The "serendipity" in this case came from the favorably immature crystallographic knowledge of this student. Knowledgeable researchers might have poled automatically according to the conventional way that the poling is conducted merely along the P_S direction, thus missing this exciting k enhancement. Another luck was good followers of our discovery; Yamashita's Group at Toshiba Corporation, Japan, promoted medical transducer developments [8], and Park and Shrout at Penn State demonstrated a large displacement generation, such as a "miracle stone" [9]. Without these followers' active developments on these single crystals, our discovery might not have been commercialized timely.

II. Electrostriction Phenomenology

After reviewing first the Devonshire phenomenology in FEs, we describe the electrostrictive couplings in the AFE case with intrasublattice and intersublattice couplings, which is directly correlated with the ionic ordering status in complex perovskite polar crystals in Section III.

A. Case of Ferroelectrics

In a perovskite FE, the paraelectric phase of which is centrosymmetric and nonpiezoelectric, the piezoelectric coupling term PX is omitted, and the "electrostrictive coupling" term P^2X is introduced as the "electromechnacal coupling." The theories for electrostriction in FEs were formulated in the 1950s by Devonshire [10] and Kay [11]. The elastic Gibbs energy can be expanded in a 1-D form

$$G_1(P, X, T) = (1/2)\alpha P^2 + (1/4)\beta P^4 + (1/6)\gamma P^6 - (1/2)sX^2 - QP^2X. \quad (1)$$

For simplicity, only α is temperature-dependent, given by $\alpha = (T - T_0)/\varepsilon_0 C$, where P, X, and T are the polarization, stress, and temperature, respectively, and C, s, and Q are called the Curie–Weiss constant, elastic compliance, and the "electrostrictive coefficient," respectively. This leads to (2) and (3)

$$E = (\partial G_1/\partial P) = \alpha P + \beta P^3 + \gamma P^5 - 2QPX \quad (2)$$

$$x = -(\partial G_1/\partial X) = sX + QP^2. \quad (3)$$

When the external stress is zero, the following set of equations are derived:

$$E = \alpha P + \beta P^3 + \gamma P^5 \quad (4)$$

$$x = QP^2 \quad (5)$$

$$1/\varepsilon_0\varepsilon = \alpha + 3\beta P^2 + 5\gamma P^4. \quad (6)$$

When the external electric field is equal to zero ($E = 0$), two different states are derived from (4): $P = 0$ and $P^2 = (-\beta + (\beta^2 - 4\alpha\gamma)^{1/2})/2\gamma$.

1) *Paraelectric Phase:* $P_S = 0$ or $P = \varepsilon_0\varepsilon E$ (under small E)

$$\text{Permittivity: } \varepsilon = C/(T - T_0)\text{(Curie–Weiss law)} \quad (7)$$

$$\text{Electrostriction: } x = Q\varepsilon_0^2\varepsilon^2E^2. \quad (8)$$

A practical electrostrictive coefficient M, defined as $x = ME^2$, is related linearly to the electrostrictive Q coefficient through

$$M = Q\varepsilon_0^2\varepsilon^2. \quad (9)$$

2) *Ferroelectric Phase:* $P_S^2 = (-\beta + (\beta^2 - 4\alpha\gamma)^{1/2})/2\gamma$ or $P = P_S + \varepsilon_0\varepsilon E$ (under small E)

$$x = Q(P_S + \varepsilon_0\varepsilon E)^2 = QP_S^2 + 2\varepsilon_0\varepsilon QP_SE + Q\varepsilon_0^2\varepsilon^2E^2 \quad (10)$$

where we define the spontaneous strain x_S and the piezoelectric constant d as

$$\text{Spontaneous strain: } x_S = QP_S^2 \quad (11)$$

$$\text{Piezoelectric constant: } d = 2\varepsilon_0\varepsilon QP_S. \quad (12)$$

For example, three independent Q reduced-matrix components, Q_{11}, Q_{12}, and Q_{44}, are considered in 3-D to discuss the paraelectric (cubic m3m)-to-FE (tetragonal) phase transition in barium titanate. In practice, Q_{11} is positive with 6.7×10^{-2} m^{4}C^{-2}, and Q_{12} is negative with -2.2×10^{-2} m^{4}C^{-2}. Thus, the spontaneous P_S and the induced polarization $\varepsilon_0\varepsilon E_3$ will generate the extension along the three axes and contraction along the perpendicular 1 and 2 axes in both phases. The Poison's ratio (estimated by $-Q_{12}/Q_{11}$) is close to 0.33 ($\sim$1/3), leading to the spontaneous volumetric expansion ($Q_h = Q_{11} + 2Q_{12} > 0$) in the FE phase.

When a hydrostatic pressure p ($X = -p$) is applied

$$\text{(Ferroelectric state)}\, 1/\varepsilon_0\varepsilon = \alpha + 3\beta P_S^2 + 5\gamma P_S^4 + 2Qp \quad (13a)$$

$$\text{(Paraelectric state)}\, 1/\varepsilon_0\varepsilon = \alpha + 2Qp = (T - T_0 + 2Q\varepsilon_0Cp)/(\varepsilon_0C). \quad (13b)$$

The inverse permittivity is changed in proportion to p. Therefore, the pressure dependence of the Curie–Weiss temperature T_0 or the transition temperature T_C is derived as follows:

$$(\partial T_0/\partial p) = (\partial T_C/\partial p) = -2Q\varepsilon_0C. \quad (14)$$

In general, the FE Curie temperature is decreased with increasing hydrostatic pressure (i.e., $Q_h > 0$). More precisely, almost the same 50 °C temperature decrease per 1 GPa hydrostatic pressure increase in most of perovskite FEs [12], leading to an important empirical rule, the "QC" constant rule, as described again in Section III.C.4.

We have discussed so far the electric-field-induced strains, i.e., piezoelectric strain (converse piezoelectric effect, $x = dE$)

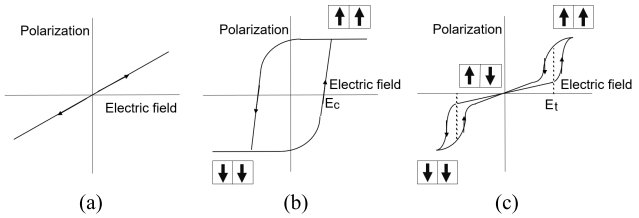

Fig. 3. Polarization versus electric field hysteresis curves in (a) paraelectric, (b) FE, and (c) AFE materials.

and electrostriction (electrostrictive effect, $x = ME^2$). Let us consider here the converse effect, that is, the material's response to an external stress, which is applicable to force sensors. The direct piezoelectric effect is the increase in the polarization by an external stress. Equation (2) provides

$$E = 2QP_S p, \quad \text{or} \Delta P = dp. \tag{15}$$

Recall (12), $d = 2\varepsilon_0 \varepsilon QP_S$.

On the contrary, since an electrostrictive material does not have a spontaneous polarization, it does not generate any charge under stress, but does exhibit a change in permittivity [derivative of (2)]

$$\Delta(1/\varepsilon_0 \varepsilon) = 2Qp \tag{16}$$

This "converse electrostrictive effect," the stress dependence of the permittivity, is used also in stress sensors [13]. A bimorph structure which subtracts the static capacitances of two dielectric ceramic plates can provide superior stress sensitivity and temperature stability. The response speed is limited by the capacitance measuring frequency to about 1 kHz. Unlike piezoelectric sensors, electrostrictive sensors are effective in the low-frequency range, especially pseudo-dc stress change.

B. Case of Antiferroelectrics

The previous sections dealt with the case in which the directions of the spontaneous dipoles are parallel to each other in a crystal (polar crystal). When the antiparallel orientation lowers the dipole-dipole interaction energy, antipolar crystals are realized. When the application of an external electric field or mechanical stress causes a transition of the dipole orientation from antiparallel to parallel state, such crystals are called "AFEs."

Fig. 3 shows the relationship between E (applied electric field) and P (induced polarization) in paraelectric, FE and AFE phases. In a paraelectric phase the P-E relation is linear [see Fig. 3(a)] under small field; in an FE phase there appears a hysteresis caused by the transition of the spontaneous polarization between the positive and negative directions [see Fig. 3(b)]; in an AFE phase, at low electric field, the induced polarization is proportional to E, and when E exceeds a certain value E_{crit}, the crystal becomes FE (electric-field-induced phase transition), and the polarization shows hysteresis with respect to E. After removal of the electric field, the crystal returns to its antipolar state, and hence, no spontaneous polarization can be observed as a whole. This is called a "double hysteresis curve" [see Fig. 3(c)].

1) Phenomenology of Antiferroelectrics: The reader probably learned the famous Kittel's phenomenology of AFEs with sublattice polarizations [14]. Though Fujimoto and Yasuda reported the "stress dependence of AFEs," their handling with the stress could not explain even the Neel temperature change trend [15]. Uchino *et al.* introduced "electrostrictive coupling" in Kittel's free energy expression for AFEs with the "two-sublattice model" [16], [17]. A superlattice (twice the unit lattice) was assumed to form two neighboring sublattices, each having a sublattice polarization P_a and P_b in 1-D expression case. The state $P_a = P_b$ represents the FE phase, while $P_a = -P_b$, the AFE phase, realized according to the η sign of the sublattice coupling energy (1/2) $\eta P_a P_b$. For the electrostrictive effect, in addition to the intrasublattice coupling between the two sublattices, where the strains are described as QP_a^2 and QP_b^2, respectively (assuming equal electrostrictive constants Q for both sublattices), the "intersublattice coupling" term qP_aP_b was introduced [17] This is the key to explain the volumetric shrinkage at the transition from paraelectric to antiferroelectic phase and the Neel temperature increase with hydraulic pressure. The elastic Gibbs energy is represented by the following form:

$$\begin{aligned} G_1 = {} & (1/4)\alpha\left(P_a^2 + P_b^2\right) + (1/8)\beta\left(P_a^4 + P_b^4\right) \\ & + (1/12)\gamma\left(P_a^6 + P_b^6\right) + (1/2)\eta P_a P_b - (1/2)\chi_T p^2 \\ & + (1/2)Q_h\left(P_a^2 + P_b^2\right) + q_h P_a P_b p \end{aligned} \tag{17}$$

where hydrostatic pressure p is employed, and χ_T is the isothermal compressibility, Q_h $(= Q_{11} + 2Q_{12})$ and q_h $(= q_{11} + 2q_{12})$ are the hydrostatic electrostrictive constants (1-D expression). Introducing the transformations $P_F = (P_a + P_b)/2$ and $P_{\mathrm{A}} = (P_a - P_b)/2$ leads to the following expression:

$$\begin{aligned} G_1 = {} & (1/2)\alpha\left(P_F^2 + P_{\mathrm{A}}^2\right) + (1/4)\beta\left(P_F^4 + P_{\mathrm{A}}^4 + 6P_F^2 P_{\mathrm{A}}^2\right) \\ & + (1/6)\gamma\left(P_F^6 + P_{\mathrm{A}}^6 + 15P_F^4 P_{\mathrm{A}}^2 + 15P_F^2 P_{\mathrm{A}}^4\right) \\ & + (1/2)\eta\left(P_F^2 - P_{\mathrm{A}}^2\right) - (1/2)\chi_T p^2 + Q_h\left(P_F^2 + P_{\mathrm{A}}^2\right) \\ & + q_h\left(P_F^2 - P_{\mathrm{A}}^2\right)p. \end{aligned} \tag{18}$$

The dielectric and elastic equations of state follow as

$$\begin{aligned} \partial G_1/\partial P_F = E = P_F\big[& \alpha + \eta + 2(Q_h + q_h)p + \beta P_F^2 + 3\beta P_{\mathrm{A}}^2 \\ & + \gamma P_F^4 + 10\gamma P_F^2 P_{\mathrm{A}}^2 + 5\gamma P_{\mathrm{A}}^4\big] \end{aligned} \tag{19}$$

$$\begin{aligned} \partial G_1/\partial P_{\mathrm{A}} = 0 = P_{\mathrm{A}}\big[& \alpha - \eta + 2(Q_h - q_h)p + \beta P_{\mathrm{A}}^2 + 3\beta P_F^2 \\ & + \gamma P_{\mathrm{A}}^4 + 10\gamma P_F^2 P_{\mathrm{A}}^2 + 5\gamma P_F^4\big] \end{aligned} \tag{20}$$

$$\begin{aligned} \partial G_1/\partial p = \Delta V/V = {} & -\chi_T p + (Q_h + q_h)P_F^2 \\ & + (Q_h - q_h)P_{\mathrm{A}}^2. \end{aligned} \tag{21}$$

Hence, the induced volume change in the paraelectric phase can be related to the induced FE polarization by the following formula:

$$(\Delta V/V)_{\mathrm{ind}} = (Q_h + q_h)P_{F,\mathrm{ind}}^2. \tag{22}$$

Below the phase transition temperature (this temperature for AFE is called "Neel temperature") the spontaneous volumetric strain and the spontaneous AFE polarization are related as

$$(\Delta V/V)_S = (Q_h - q_h)P_{A,S}^2. \tag{23}$$

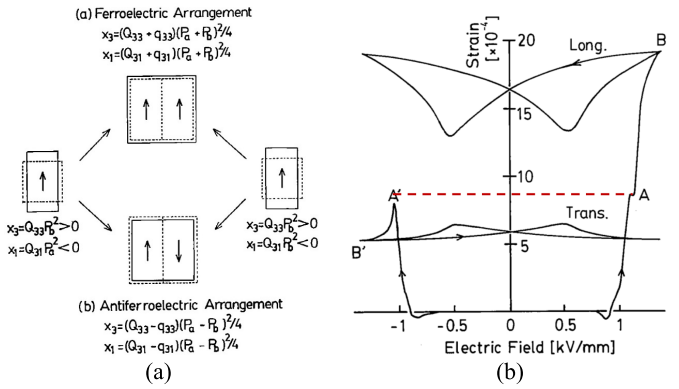

Fig. 4. (a) Spontaneous strain changes in 3-D associated with sublattice interactions in the electrostrictive effect. The illustration is drawn in the case of q_{33} and $q_{31} > 0$. (b) Longitudinal and transverse induced strains in the sample $Pb_{0.99}Nb_{0.02}[(Zr_{0.6}Sn_{0.4})_{0.925}Ti_{0.075}]_{0.98}O_3$ [18].

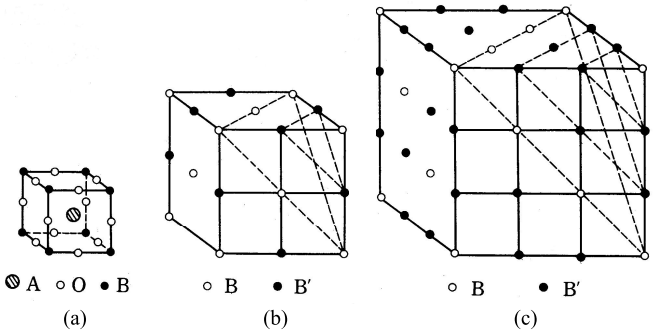

Fig. 5. Ordered arrangements of B-site ions in complex perovskites: (a) simple type (ABO_3), (b) 1:1 order type ($AB_{1/2}B'_{1/2}O_3$), and (c) 1:2 order type ($AB_{1/3}B'_{2/3}O_3$).

Even if the perovskite crystal shows $Q_h > 0$, the spontaneous volumetric strain can be positive or negative depending on the value of $q_h (q_h < Q_h$ or $q_h > Q_h)$, that is, if the intersublattice coupling is stronger than the intrasublattice coupling (i.e., $q_h > Q_h$), a volume contraction is observed at the Neel point (more popular in AFE). This is quite different from FEs, which always show a volume expansion at the Curie point, because $Q_h > 0$. When P_a and P_b are in the parallel configuration (FE phase), the q_h acts to increase the strain x_S, when they are in the antiparallel configuration (AFE phase), the q_h acts to decrease the strain. The large change in the strain associated with the field-induced transition from the AFE to FE phase can be estimated to be

$$\begin{aligned}(\Delta V/V) &= (\Delta V/V)_{\text{ind}} - (\Delta V/V)_S \\ &= (Q_h + q_h)P_{F,S}^2 - (Q_h - q_h)P_{A,S}^2 \\ &= 2\, q_h P_{F,S}^2. \end{aligned} \tag{24}$$

Here, we assume that the magnitudes of P_a and P_b do not change drastically through the phase transition; that is, $P_{F,S} \approx P_{A,S}$.

This phenomenological theory explains well the experimental results for the AFE perovskite $PbZrO_3$-based ceramics by extending it to 3-D [18], [19]. Suppose P_a and P_b along the three axes, the 3-D strain changes associated with the E_3 field-induced transition from AFE to FE are probably given by

$$\Delta x_3 = (Q_{33} + q_{33})P_{F3}^2 - (Q_{33} - q_{33})P_{A3}^2 = 2q_{33}P_{F3}^2 \tag{25a}$$

$$\Delta x_1 = \Delta x_2 = (Q_{31} + q_{31})P_{F3}^2 - (Q_{31} - q_{31})P_{A3}^2 = 2q_{31}P_{F3}^2. \tag{25b}$$

Here, $P_{F3} = P_{A3}$ was also assumed because only the flipping of polarizations P_a and P_b would occur at the transition. Fig. 4(a) illustrates the spontaneous strain changes in 3-D associated with sublattice interactions in the electrostrictive effect. Illustration is drawn in the case of q_{33} and $q_{31} > 0$, while Fig. 4(b) plots the longitudinal (L)- and transverse (T)-induced strains in the sample $Pb_{0.99}Nb_{0.02}[(Zr_{0.6}Sn_{0.4})_{0.925}Ti_{0.075}]_{0.98}O_3$ [PNZST]. Note that the strain curves for L and T are plotted mirror-symmetrically with respect to the field E to show the strain jump curves clearly. With increasing the electric field, both L and T strains are almost zero in the AFE state. Around $E = 1$ kV/mm (-1 kV/mm in the T curve), both strains jump suddenly by 8×10^{-4} (i.e., large "isotropic expansion"!), relating to the AFE-to-FE transition, denoted as A and A' in Fig. 4(b). Then, additional extension by 10×10^{-4} longitudinally (A→B) and transverse contraction by -3×10^{-4} follow (A'→B') with slight time lag due to the FE domain reorientation. Once the electrically poled state is induced in the specimen ceramic, typical butterfly-shape L and T strain curves are observed during the electric field cycle.

2) Piezoelectric Anisotropy: The intersublattice coupling q_{33} and q_{31} values were evaluated using experimental strains and polarization data for PNZST reported in [18] and [19] and $\delta T_N/\delta p$ of the $PbZrO_3$-based sample [12]

$$\begin{aligned} P_{F3} &= P_{A3} = 0.4\left(\text{C}\cdot\text{m}^{-2}\right); \quad \Delta x_3 = \Delta x_1 = 8 \times 10^{-4} \\ Q_h &= Q_{33} + 2Q_{31} = 0.5 \times 10^{-2}\left(\text{m}^4\cdot\text{C}^{-2}\right) \\ q_h &= q_{33} + 2q_{31} = 0.9 \times 10^{-2}\left(\text{m}^4\cdot\text{C}^{-2}\right). \end{aligned}$$

Then, we derive the following results:

$$\begin{aligned} Q_{33} &= 1.5\times10^{-2}\left(\text{m}^4\cdot\text{C}^{-2}\right), \quad Q_{31} = -0.5\times10^{-2}\left(\text{m}^4\cdot\text{C}^{-2}\right) \\ q_{33} &= 0.3\times10^{-2}\left(\text{m}^4\cdot\text{C}^{-2}\right), \quad q_{31} = 0.3\times10^{-2}\left(\text{m}^4\cdot\text{C}^{-2}\right). \end{aligned}$$

It is noteworthy that q_{33} and q_{31} have the same positive sign (accidentally almost the same value), while Q_{33} and Q_{31} have the opposite sign showing a normal "piezoelectric Poisson's" ratio of 1/3. The theoretical explanation on the "negative Poisson's ratio" (i.e., isotropic volumetric expansion) among the intersublattice coupling q_{33} and q_{31} is a future problem to be solved since phenomenological advancement has not been seen after the Uchino group's studies above. This intersublattice electrostrictive coupling factors can explain successfully a very small d_{31} and an enormous piezoelectric anisotropy $|d_{33}/d_{31}| \approx 9$ in some PT-rich PZT compositions [20], [21], which is preferable to ultrasonic medical probe applications [22], [23].

III. Complex Perovskites

A. Tolerance Factor

"Perovskite" type oxides [ABO_3 in Fig. 5(a)] are our primary targets to develop superior FE/piezoelectric materials

because this structure can exhibit enormous Lorentz factor γ, such as ~10 for barium titante [24], so that large "local field" and "dipole coupling energy" (i.e., feedback force to realize the ionic shift or dipole moment in a crystal lattice) are expected. Not all ABO_3 compounds can exhibit the perovskite structure with an oxygen-octahedron-corner-sharing type but, sometimes, different structures, such as $LiNbO_3$ in an ilmenite-like octahedron-face-sharing puckered type with a small Li ion. In order to create the perovskite structure, A and B ion sizes are primarily important. For closed-shell A and B ions, the "tolerance factor"

$$t \equiv \frac{r_A + r_O}{\sqrt{2}(r_B + r_O)} \tag{26}$$

(r_A, r_B, and r_O denote the ionic radius of A, B, and O ions) is frequency used to discuss the Perovskite structure stability [25]. The case $t = 1$ means that three ions are closely packed each other, while $t > 1$ and $t < 1$ cases stand for the existence of rattling space around the B and A ions, respectively. Empirically, $t > 0.855$ seems to be a threshold to maintain the perovskite structure, below which too small A ion (such as Li) introduces a puckered structure. However, the ferroelectricity is not predicted directly by the tolerance factor but by the ionic size of B ion dominantly. Its size 0.6–0.7 Å seems to be preferable to introduce polar or antipolar status. The discussion of Pb^{2+} ion ($PbTiO_3$) with nonclosed-shell ion configuration is not so simple as Ba^{2+} ($BaTiO_3$) with a similar closed-shell ionic configuration to [Xe^{54}], in which we need to consider nonspherical 5d electron orbital interaction with the adjacent oxygen ions.

B. Ionic Ordering and Ferroelectricity

This article focuses on relaxor perovskite FEs with complex perovskites of a combination of different valence B ions with keeping the average valence as +4, such as $A^{2+}(B^{2+}_{1/2}B^{6+}_{1/2})O_3$, $A^{2+}(B^{3+}_{1/2}B^{5+}_{1/2})O_3$, and $A^{2+}(B^{2+}_{1/3}B^{5+}_{2/3})O_3$.

Let us take some examples of complex perovskites: $Pb(Mg_{1/3}Nb_{2/3})O_3$, $Pb(Mg_{1/2}W_{1/2})O_3$, and $Ba(Mg_{1/3}Ta_{2/3})O_3$. First, $Pb(Mg_{1/3}Nb_{2/3})O_3$ exhibits "random arrangement" of Mg^{2+} and Nb^{5+} ions on the B-sites and is called a "disordered" perovskite, which is equivalent to a simple perovskite [see Fig. 5(a)] from the macroscopic crystal structure's viewpoint. We should point out the "short-range ionic ordering" in this material, which exhibits microscopic mixed regions of random and ordered arrangement ("Kanzig regions") [70], [71], as discussed in Section VII-B. Second, $Pb(Mg_{1/2}W_{1/2})O_3$ shows an "ordered" arrangement of Mg^{2+} and W^{6+} in an NaCl-type, as shown in Fig. 5(b) (1:1 order). Third, the cation ordering is also found in $Ba(Mg_{1/3}Ta_{2/3})O_3$, where Mg^{2+} and Ta^{5+} are arranged in the sequence of Mg–Ta–Ta in the ⟨111⟩ direction [1:2 order; see Fig. 5(c)] [26]. The degree of the ionic ordering in complex perovskites depends basically on the difference in the valence charge and/or in the ionic radius, which provides the sum of Madelung energy, polarization, and displacement (elastic) energy [27].

The ordering of the ionic arrangement gives a significant effect on ferroelectricity. Simple perovskites exhibit either ferroelectricity ($BaTiO_3$ and $PbTiO_3$) or antiferroelectricity ($PbZrO_3$ and $PbHfO_3$). On the other hand, the 1:1 ordered complex perovskites tend to be antiFE ($Pb(Mg_{1/2}W_{1/2})O_3$ and $Pb(Co_{1/2}W_{1/2})O_3$), which may be due to the intersublattice coupling enhancement, while disordered perovskites tend to be FE ($Pb(Mg_{1/3}Nb_{2/3})O_3$ and $Pb(Fe_{1/2}Ta_{1/2})O_3$). In addition, the phase transition of the "disordered perovskite" is rather diffused, and the crystal structure in the low temperature phase is rhombohedral, rather than tetragonal in $BaTiO_3$ and $PbTiO_3$.

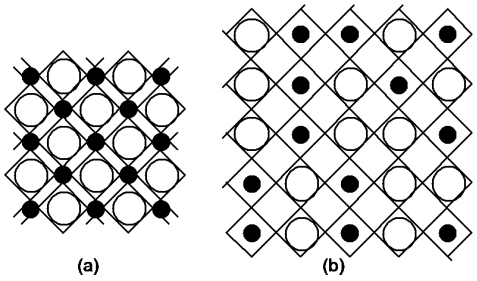

Fig. 6. Crystal structure models of the $A(B_{I,1/2}B_{II,1/2})O_3$ type perovskite: (a) ordered structure with a small rattling space and (b) disordered structure with a large rattling space [$O = B_I$ and $\bullet = B_{II}$].

The close relationship between dielectric and crystallographic properties is suggestively exemplified in the previous work on $Pb(Sc_{1/2}Ta_{1/2})O_3$ (PST) by Setter and Cross [28]. The degree of the cation ordering (Sc^{3+}, Ta^{5+}) was manipulated by simple thermal annealing without any composition change. They reported the differences in the dielectric constant and the spontaneous polarization in different ion-order levels. The disordered sample (ordering parameter $S = 0.35$) exhibits a "diffuse transition" from an FE to a paraelectric phase. With increasing the ordering level ($S = 0.80$), the phase transition becomes "sharp" and occurs at a higher temperature (i.e., the polar state is more stable). This partially ordered PSN exhibited paraelectic-to-FE phase transition, without showing the AFE phase. Though various papers can be found on the ion-ordering principle, clear explanation on the relationship with ferroelectricity has not been made yet.

It is interesting to mention that the materials with the 1:2 cation order are usually nonpolar (NP), and often applicable to microwave dielectrics (i.e., now electromagnetic interaction up to the GHz range) [29].

C. QC Constant Rule

1) Rattling Ion Model: An intuitive crystallographic model (i.e., "rattling ion model") was proposed first by Uchino *et al.* [3], [30] to explain enormous permittivity, small electrostrictive coefficient Q ($\Delta x = Q P^2$), and large electrostrictive constant M ($\Delta x = M E^2$) in the disordered perovskites. Fig. 6(a) and (b) shows the ordered and disordered structures for an $A(B_{I,1/2}B_{II,1/2})O_3$ perovskite crystal (B_I is a larger ion than B_{II}). Assuming a rigid ion model, a large "rattling" space is expected for the smaller B_{II} ions in the disordered structure [see Fig. 6(b)] because the large B_I ions prop-open the lattice framework. On the contrary, much less "rattling" space is expected in the ordered arrangement [see Fig. 6(a)] where neighboring atoms collapse systematically around the small

TABLE I
ELECTROSTRICTIVE COEFFICIENTS Q_h, CURIE–WEISS CONSTANTS C, AND THEIR PRODUCT VALUES

Order-type	Polar-type	Substance	Q_h ($\times 10^{-2}$ m^4 C^{-2})	C^{eff} ($\times 10^5$ K)	$Q_h C$ ($\times 10^3$ m^4 C^{-2} K)
Disorder	Ferroelectric	$Pb(Mg_{1/3}Nb_{2/3})O_3$	0.60	4.7	2.8
		$Pb(Zn_{1/3}Nb_{2/3})O_3$	0.66	4.7	3.1
	Non-polar	$(K_{3/4}Bi_{1/4})(Zn_{1/6}Nb_{5/6})O_3$	0.55–1.15	–	–
Partial-order	Ferroelectric	$Pb(Sc_{1/2}Nb_{1/2})O_3$	0.83	3.5	2.9
	Antiferroelectric	$Pb(Fe_{2/3}U_{1/3})O_3$	–	2.3	–
Order	Antiferroelectric	$Pb(Co_{1/2}W_{1/2})O_3$	–	1.2	–
		$Pb(Mg_{1/2}W_{1/2})O_3$	6.2	0.42	2.6
Simple	Ferroelectric	$BaTiO_3$	2.0	1.5	3.0
		$PbTiO_3$	2.2	1.7	3.7
		$SrTiO_3$	4.7	0.77	3.6
		$KTaO_3$	5.2	0.5	2.6
	Antiferroelectric	$PbZrO_3$	2.0	1.6	3.2
	Non-polar	$BaZrO_3$	2.3	–	–

B_{II} ions. The densely packed structure in Fig. 6(a) has actually been observed by Amin *et al.* [31] for $Pb(Mg_{1/2}W_{1/2})O_3$-based ceramics.

2) Dielectric Permittivity: When an electric field is applied to a disordered perovskite, the small B_{II} ions (usually higher valence ions) with a large rattling space can shift easily without distorting the oxygen framework. Larger polarization can be expected for unit magnitude of electric field; in other words, since permittivity is defined by $\varepsilon_0\varepsilon = \partial P/\partial E$, larger dielectric constants (or larger Curie–Weiss constants in the case of FEs) are expected in this case. On the other hand, in ordered perovskites with a very small rattling space, neither B_I nor B_{II} ions can move easily without distorting the octahedron. A smaller permittivity and a smaller Curie–Weiss constant are expected.

3) Electrostrictive Coefficient: When an electric field is applied to a disordered perovskite, the small B_{II} ions with a large rattling space can shift easily without distorting the oxygen framework. Since the induced polarization is large for a certain lattice frame distortion (i.e., strain), we can expect a small electrostriction coefficient Q defined by $x = QP^2$. On the other hand, in ordered perovskites with a very small rattling space, neither B_I nor B_{II} ions can move easily without distorting the octahedron. Q should be large because small polarization generates a certain lattice frame distortion.

4) QC Constant Rule: Hydrostatic electrostriction coefficients Q_h $(= Q_{11} + 2Q_{12})$ and Curie–Weiss constants C (determined from the average slope of the $1/\varepsilon$–T curve in the $(T - T_C) < 100°$ range) for several kinds of perovskite-type oxide crystals are summarized in Table I according to a paper by Uchino *et al.* [3]. Coefficients are listed for disordered, partially ordered, ordered, and simple perovskite FE, AFE, and NP dielectric substances. Refer to [2] and [30] for data sources. Multiple empirical rules from this table were proposed.

Rule 1: The magnitude of the electrostrictive coefficient is not affected strongly by FE, AFE, or NP characteristics but is dependent primarily on the degree of ionic order. The electrostrictive coefficient Q increases with cation order from disordered through partially ordered, simple, and then ordered perovskites.

Rule 2: The Curie–Weiss constant decreases in accordance with disordered, though partially ordered, simple, and then, finally, ordered.

Rule 3: The product of electrostriction coefficient Q and the Curie–Weiss constant C is nearly constant for all FE and AFE perovskites $Q_hC = 3.1(\pm 0.4) \times 10^3$ m^{4}C^{-2}K].

An intuitive explanation of these rules by the "rattling ion model" is discussed in more detail in Section VI-B. Note that small Q does not mean small electrostriction induced in relaxor FEs. Knowing $P = \varepsilon_0\varepsilon E$, since $x = Q(\varepsilon_0\varepsilon)^2E^2$, we obtain $M = Q(\varepsilon_0\varepsilon)^2$. Using the above rule $Q\varepsilon \approx$ constant, giant electrostriction is anticipated for disordered perovskite FEs because of large permittivity ε.

Though the "QC constant rule" seems to be an elegant and universal rule, there remain several critical arguments in the disordered relaxor FEs.

1) *Overestimated Curie–Weiss Constant in This Table:* The real linearity of the $1/\varepsilon$–T curve is observed at very high temperature $T > 600$ K. $C = 1.2 \times 10^5$ K was reported by Poplavko *et al.* [32] and Viehland *et al.* [33] for single

and ceramics PMN, respectively. Toulouse reported $C = 2.2 \times 10^5$ K for PZN crystals [34].

2) *Incorrect Argument in Rule 2:* Stenger and Burggraaf [35] reported $C = 1.5 \times 10^5$ K for both disordered and ordered PST single-crystal specimens introduced previously. Furthermore, Lei *et al.* [36] reported a significant decrease in C with increasing disorder levels. The reader can refer to a comprehensive review paper by Li *et al.* [37].

However, it seems too early to abandon the above empirical "$Q \cdot C$ constant rule." The "intrinsic" Curie–Weiss constant determined from very high temperature $T > 600$ K may not be relevant to use in this table. Since the giant electrostriction is observed just above the Curie temperature, the values of Q and C should be determined in the same discussing temperature range, where the $1/\varepsilon$–T curve does not follow the normal Curie–Weiss law but the modified critical exponent formula, as discussed in Section VII. Therefore, the average slope of $1/\varepsilon$ was used as the "effective Curie–Weiss constant," instead of the "true" Curie–Weiss constant, in Table I. We first need to wait for the electrostrictive Q coefficient determination in the same temperature range ($T > 600$ K). Second, taking the "polar nanoregion" (PNR) existence into account, a new theoretical approach may be required to correlate the Curie–Weiss-like constant C' with critical exponent γ with the giant electrostriction with the small Q. As discussed in Section VII, isotropic statistical models, such as Gaussian distribution by Rolov [54] and the well-accepted Vogel–Fulcher model, are not quite satisfactory for deriving the exponent parameter γ.

IV. Microscopic Origin of Electrostriction

A. Born Ionic Model

Piezoelectricity is derived from the difference between two harmonic (linear) springs in an asymmetric crystal, while the electrostriction is originated from the anharmonic (nonlinear) springs in a centrosymmetric crystal [38]. Uchino and Cross [40] derived the electrostriction coefficient numerically from the Born model [39], which proposed the theory of cohesive forces in ionic crystals in the simplest two-ion rock-salt structure. The potential function involves an inverse power type of repulsive quantum-mechanical energy and the Coulombic energy in a 1-D spherical model, as illustrated in Fig. 7

$$U = -\frac{Mq^2}{r} + \frac{Nb}{r^n} \tag{27}$$

where M is the "Madelung constant" for Coulombic energy, instead of merely the nearest neighbor's interaction, in order to take into account all crystal lattice periodic atoms. On the other hand, N in the second term is the coordination number, and b is a potential constant for quantum mechanical energy. We assume a relatively large number 9–11 for n in quantum mechanical repulsive potential $1/r^n$. Expanding the potential function (including the first anharmonic term) around the equilibrium position ($r_0^{n-1} = nNb/Mq^2$ from the condition $(\partial U/\partial r) = 0$), we obtain the form as a function of Δr $(= r - r_0)$

$$\Delta U = U(r) - U(r_0) = f(\Delta r)^2 - g(\Delta r)^3 \tag{28}$$

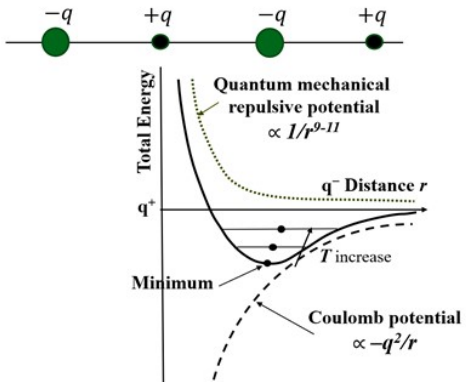

Fig. 7. 1-D ionic crystal model by Born for a two-ion rock-salt structure.

where $f = (n-1)Mq^2/2r_0^3$ and $g = (n+4)(n-1)Mq^2/6r_0^4$. It is essential to realize the curvature difference in the positive and negative regions of Δr, that is, the lattice spring is softer for extension than for contraction. The negative sign in front of g is for keeping positive g in (28).

B. Thermal Expansion and Electrostriction

The ionic displacement Δr is supposed to be generated under a small electric field (E) applied and under a finite temperature (T). Using the Boltzmann distribution for Gibbs energy $\Delta V_\pm = \Delta U \pm qE\Delta r$ under the applied electric field E, the average equilibrium separation at an elevated temperature is approximated as follows:

$$\langle \Delta r_\pm \rangle \sim \int_{-\infty}^{\infty} \Delta r \exp\left(-\frac{\Delta V_\pm}{k_B T}\right) d\Delta r \Big/ \int_{-\infty}^{\infty} \exp\left(-\frac{\Delta V_\pm}{k_B T}\right) d\Delta r$$
$$\sim \frac{3gk_B}{4f^2} T \pm \frac{q}{2f} E + \frac{3gq^2}{4f^3} E^2 \tag{29}$$

where subscripts $\pm$ denote the position shifts for ion pairs (Na^{+1} and Cl^{-1}) in terms of the electric field, respectively (i.e., opposite direction due to the charge difference $+q$ and $-q$). Refer to [41] and [42] for the derivation process.

First, the polarization P is obtained from the harmonic term and given by

$$P = \frac{q\langle \Delta r \rangle}{2r_0^3} = \frac{q^2}{4fr_0^3} E. \tag{30a}$$

Thus, the permittivity is evaluated as

$$\varepsilon_0 \varepsilon = \frac{q^2}{4fr_0^3}. \tag{30b}$$

Next, the strain is given by the summation of the shifts

$$\frac{\langle \Delta r_+ \rangle + \langle \Delta r_- \rangle}{2r_0} = \frac{3gk_B}{4f^2 r_0} T + \frac{3gq^2}{4f^3 r_0} E^2 \tag{31}$$

where the first term represents the thermal expansion and the second term represents the electrostriction (no piezoelectricity is expected in this cubic symmetry). Note that the second term in (29), $\pm(q/2f)E$, corresponding to the absolute position shifts of Na^{+1} and Cl^{-1}, which is in the same magnitude in the opposite direction, does not contribute to the crystal lattice strain! Fig. 7 visualizes the $-q$ ion average position

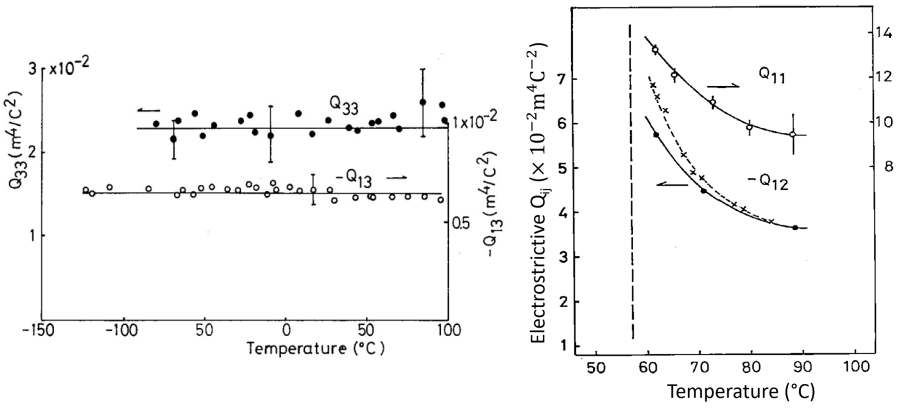

Fig. 8. Temperature dependence of the electrostrictive constants Q_{33} (Q_{11}) and Q_{13} (Q_{12}) measured in single crystals (a) $Pb(Mg_{1/3}Nb_{2/3})O_3$ and (b) $K(Ta_{0.55}Nb_{0.45})O_3$.

drift (with respect to $+q$ position) with elevating temperature. Because of the softer lattice spring performance for extension, thermal expansion (i.e., positive strain) is generally observed. The reader can understand that both thermal expansion and electrostrictive coefficients are originated from "g," which is an anharmonic term $g(\Delta r)^3$ in (29), and neither thermal expansion nor electrostriction occurs when the crystal is purely harmonic [that is, only $f(\Delta r)^2$ term in (29)]. Knowing the polarization P, given by (30a), the thermal expansion coefficient α_L and electrostrictive Q coefficient (defined by $(\Delta r/r) = QP^2$) can be described with atomic parameters in the Born model as

$$\alpha_L = \frac{3gk_B}{4f^2r_0} = \frac{(n+4)k_B}{2n(n-1)Nb}r_0^n \tag{32}$$

$$Q = \left(\frac{3gq^2}{4f^3r_0}\right)/\left(\frac{q^2}{4fr_0^3}\right)^2 = \frac{4(n+4)M}{nNb}r_0^{n+3} \tag{33}$$

where k_B and M are Boltzmann and Madelung constants, respectively. If we suppose that M and the potential constant b are relatively insensitive to materials, and r_0 is the primary variable, we obtain

$$\alpha_L \propto Q^{n/(n+3)}. \tag{34}$$

Uchino and Cross [40] reported a good correlation between α_L and Q among various ionic crystals as $\alpha_L = 4.2 \times 10^{-5} Q_h^{0.5}$ (correlation coefficient $r = 0.94$). Equation (34) seems to be reasonable if $n \sim 34$. However, this result is inconsistent with the usually accepted value $n \sim 811$. More advanced models will clearly be desired to explain the observed relationship.

Note that the above derivation of electrostriction conducted from the lattice anharmonicity is not directly related to the giant electrostriction in relaxor FEs composed of polar nanodomains.

V. Experimentation of Electrostriction

A. Electrostriction Characterization Methods

We treat the electrostrictive coefficient as a temperature-independent constant in most of the phenomenological theories. What is the actual situation? Several expressions for the electrostrictive coefficient Q have been given so far, which indicates the following experimental methods, knowing the spontaneous P_S and/or permittivity ε beforehand.

1) Electric-field-induced strain (i.e., electrostriction) in the paraelectric phase ($x = QP_{\text{ind}}^2$ or $x = Q(\varepsilon_0\varepsilon)^2E^2$).
2) Spontaneous polarization P_S and spontaneous strain x_S (determined via X-ray diffraction) in the FE phase ($x_S = QP_S^2$).
3) d constants from the field-induced strain (piezostriction) in the FE phase or measured by the piezoelectric resonance technique; d constants from the polarization induced by the external stress in the FE phase ($d = 2Q\varepsilon_0\varepsilon P_S$).
4) Hydrostatic pressure dependence of inverse permittivity in the paraelectric phase ($\partial((1/\varepsilon_0\varepsilon))/\partial p = 2Q_h = Q_{11} + 2Q_{12}$). We use Poisson's ratio $\sigma = -Q_{12}/Q_{11} = 1/3$ for evaluating individual Q values.

B. Experimental Results of Electrostrictive Coefficients

1) $Pb(Mg_{1/3}Nb_{2/3})O_3$: Fig. 8(a) shows the temperature dependence of the electrostrictive coefficients Q_{33} and Q_{13} observed for a complex perovskite $Pb(Mg_{1/3}Nb_{2/3})O_3$ (PMN) ceramic sample, whose Curie temperature is near 0 °C [43]. The result in a single-crystal value shows very close data (slightly higher than the polycrystalline specimen) [2]. Experimental methods 1), 3), and 4) provided almost the same values, which are plotted together in this figure. It is seen that there is no significant anomaly in the electrostrictive coefficient Q through the temperature range in which the paraelectric-to-FE phase transition occurs and piezoelectricity appears. Q seems to be almost temperature-independent in relaxor FEs in this temperature range (−100 °C∼100 °C).

2) $K(Ta_{0.55}Nb_{0.45})O_3$: The electrostrictive coefficients Q_{11} and Q_{12} observed in a single crystal $K(Ta_{0.55}Nb_{0.45})O_3$(KTN) specimen are shown in Fig. 8(b) as a function of temperature [via the experimental method (1)] [44]. The dashed line was estimated from $x_2 = Q_{12}\varepsilon_0^2\varepsilon_1^2E_1^2$ with the weak-field permittivity. Note that we use Q_{33} and Q_{13} for ceramic specimens and Q_{11} and Q_{12} for single-crystal specimens conventionally

even in the same cubic crystals. Different from PMN, the KTN exhibits significant temperature dependence in the paraelectric phase. The almost saturated values at 90 °C, $Q_{11} = 9.5 \times 10^{-2}$ m^{4}C^{-2}, and $Q_{12} = -3.6 \times 10^{-2}$ m^{4}C^{-2} are close to the electrostrictive coefficients of the end members, $KTaO_3$ [45] and $KNbO_3$ [46]. However, the Q coefficients reveal a remarkable increase with decreasing temperature down to the Curie point of 57 °C. In parallel, we found some anomalies in the temperature dependence of dielectric permittivity (discussed again in Section VII-C1). In the paraelectric phase, the inverse permittivity started to deviate from the linear Curie–Weiss plot with decreasing temperature in the temperature range $T - T_C < 30$ °C; this corresponds exactly to the temperature range where the electrostrictive coefficients show a significant anomaly.

C. Polarization Fluctuation Consideration

The above anomalies in the electrostrictive coefficient and permittivity in KTN suggest a kind of critical phenomenon associated with the phase transition. Uchino *et al.* [44] proposed a simple polarization critical-fluctuation model for explaining the anomaly just above the Curie temperature. A polarization fluctuation by lattice vibration at a temperature T can be described as

$$P_i = \langle P_i \rangle + \Delta P_i \text{(Subscript } i \text{ refers to 3-D components)} \tag{35}$$

where $\langle P_i \rangle$ means the averaged polarization under experimental measurement frequency (pseudo-dc), while ΔP_i a deviation from the average (at infrared frequency, 10^{12} Hz). Thus, $\langle \Delta P_i \rangle = 0$ is expected in the measurement.

When an electric field is applied on a cubic crystal along one axis, and two and three directions are equivalent, the averaged electrostriction $\langle x_1 \rangle$ and $\langle x_2 \rangle$ can be calculated as

$$\begin{aligned}\langle x_1 \rangle &= Q_{11}\langle P_1^2 \rangle + 2Q_{12}\langle P_2^2 \rangle \\ &= Q_{11}\left[\langle P_1 \rangle^2 + \langle (\Delta P_1)^2 \rangle\right] + 2Q_{12}\langle (P_2)^2 \rangle \\ \langle x_2 \rangle &= Q_{12}\langle P_1^2 \rangle + (Q_{11} + Q_{12})\langle P_2^2 \rangle \\ &= Q_{12}\left[\langle P_1 \rangle^2 + \langle (P_1)^2 \rangle\right] + (Q_{11} + Q_{12})\langle (P_2)^2 \rangle.\end{aligned}$$

The polarization fluctuation terms $\langle (\Delta P_i)^2 \rangle$ are essential to the secondary effect (the electrostriction effect); which is very different from the situation in the primary effect (the piezoelectric effect), where the polarization fluctuations are canceled out (i.e., $\langle \Delta P_i \rangle = 0$!). Since the observed electrostrictive coefficients Q^{obs}'s are usually calculated on the basis of the average strain $\langle x_i \rangle$ and polarization $\langle P_i \rangle$ at pseudo-dc, the following experimental equations are obtained:

$$\begin{aligned}Q_{11}^{\text{obs}} &= \frac{\langle x_i \rangle}{\langle P_1 \rangle^2} = Q_{11}\left[1 + \langle (\Delta P_1)^2 \rangle / \langle P_1 \rangle^2\right] \\ &\quad + 2Q_{12}\langle (\Delta P_2)^2 \rangle / \langle P_1 \rangle^2 \qquad (36a) \\ Q_{12}^{\text{obs}} &= \frac{\langle x_2 \rangle}{\langle P_1 \rangle^2} = Q_{12}\left[1 + \langle (\Delta P_1)^2 \rangle / \langle P_1 \rangle^2\right] \\ &\quad + (Q_{11} + Q_{12})\langle (\Delta P_2)^2 \rangle / \langle P_1 \rangle^2. \qquad (36b)\end{aligned}$$

Supposing that $\langle (\Delta P_1)^2 \rangle > \langle (\Delta P_2)^2 \rangle$, Q^{obs} is characterized by the term $[1 + \langle (\Delta P_1)^2 \rangle / \langle P_1 \rangle^2]$. If the polarization fluctuation $\langle (\Delta P_1)^2 \rangle$ diverges due to the "mode softening" when approaching the phase transition from a higher temperature, the anomaly of Q^{obs}'s in the vicinity of the transition can be clearly explained. Naturally, at sufficiently higher temperatures, Q^{obs} will approach Q_{11} or Q_{12} because $\langle (\Delta P_1)^2 \rangle \to 0$. It is worth noting that the intrinsic electrostrictive coefficients Q_{11} and Q_{12} maybe insensitive to temperature in this model. Only the pseudostatic experimental technique can detect the significant temperature dependence of Q^{obs}'s due to the "polarization fluctuation."

Though this type of Q^{obs} anomaly might be observed generally in any FE material near its phase transition temperature, the observed magnitude may depend on the nature of each material. In the case of $Pb(Mg_{1/3}Nb_{2/3})O_3$, for instance, a very diffused phase transition characteristic seems to broaden the electrostrictive anomaly, making it difficult to be detected, that is, $\langle (\Delta P_1)^2 \rangle$ will not diminish up to a very high temperature.

VI. Anharmonicity in Relaxor Ferroelectrics

A. Lyddane–Sachs–Teller Relation

The lattice vibration analysis is used occasionally for discussing the electrostrictive and FE phase transition from the soft-phonon viewpoint. Refer to [41] and [42] for the fundamental derivation of the lattice vibration formulae on the 1-D two-ion model. Taking into account the external ac electric field (at ω) effect on the lattice vibration, the permittivity formula in terms of the eigenfrequencies was derived in $BaTiO_3$ by Cochran [47] and Kurosawa [48], which may be applied basically for other isomorphic perovskite FEs.

Knowing a general definition of permittivity: $D = \varepsilon_0 E + P = \varepsilon_0 \varepsilon E$ (D: electric displacement), we express the polarization P composed of electronic and ionic contributions: $P = P_{\text{ele}} + P_{\text{ion}}$. Taking a high-frequency permittivity originated from the average electronic polarizability as ε_{ele} (we also denote ε_∞), the total polarization is expressed by adding the ionic polarization as

$$P = \varepsilon_0(\varepsilon_{\text{ele}} - 1)E + N\sum_{i=1}^{5} e_i^* u_i \qquad \left[\text{charge neutralization condition, } \sum_{i=1}^{5} e_i^* = 0\right] \tag{37}$$

where i stands for the ion number for $BaTiO_3$ [Ba = 1, Ti = 2, $O_I = 3$, $O_{II} = 4$, and $O_{III} = 5$ (top and bottom of Ti)], N is the number of the unit cells per unit volume, e_i^* is the effective ionic charge (slightly deviated from Ba^{2+}, Ti^{4+}, and O^{2-}), and u_i is the displacement of the i ion, which is coupled with the lattice vibration.

Using the elastic stiffness c_{ij} (equivalent to the spring constant K), the displacement u_i should satisfy

$$\sum_{j=1}^{5} c_{ij} u_j = e_i^* E. \tag{38}$$

Note that the subscripts of c_{ij} here do not stand for the coordinate (1, 2, or 3) but, for the ion number $(1, 2, \ldots, 5)$. That is, five springs ate connected with one ion. Suppose that the ion displacement is given by $u_i^0(\omega)\cdot e^{j\omega t}$ and polarization $\mathrm{P}e^{j\omega t}$ (no delay or loss) under ac electric field $Ee^{j\omega t}$ applied (without time lag or loss); the dynamic equation for the ith ion (mass M_i) is given by

$$\sum_{j=1}^{5} c_{ij}u_j^0(\omega) - M_i\omega^2 u_i^0(\omega) = e_i^* E. \tag{39}$$

Once we integrate $u_i^0(\omega)$ from (39), we obtain the permittivity in terms of lattice model parameters

$$\varepsilon = \varepsilon_{\mathrm{ele}} + \frac{N}{\varepsilon_0 E}\sum_{i=1}^{5} e_i^* u_i^0(\omega). \tag{40}$$

Expanding the atomic chain lattice model into 3-D, we consider "transverse waves," in addition to "longitudinal waves." The reader is reminded of the fact that for a wavelength much longer than the lattice unit but smaller than the specimen size (~10 mm), which corresponds wave vector $k \approx 0$, the following boundary conditions occur for the transverse and longitudinal waves:

$$\text{Longitudinal (L) wave: } D = 0, \quad E = -P/\varepsilon_0 \tag{41a}$$

$$\text{Transverse (T) wave: } E = 0, \quad D = P. \tag{41b}$$

Accordingly, (39) is solved in two ways.

1) *Longitudinal Wave–Eigenfrequency Ω_L:*

$$\sum_{j=1}^{5} c_{ij}u_j - M_i\Omega_L^2 u_i = -e_i^* P/\varepsilon_0. \tag{42}$$

Taking $P = (N/\varepsilon_0)\sum_{i=1}^{5} e_i^* u_i$ into account, the solving equation becomes

$$\sum_{j=1}^{5} c_{ij}u_j + \frac{N}{\varepsilon_0^2} e_i^* \sum_{j=1}^{5} e_j^* u_j - M_i\Omega_L^2 u_i = 0. \tag{43}$$

2) *Transverse wave–Eigenfrequency Ω_T:*

$$\sum_{j=1}^{5} c_{ij}u_j - M_i\Omega_T^2 u_i = 0. \tag{44}$$

Introducing (43) and (44) into (40), we can obtain the permittivity in terms of Ω_L and Ω_T

$$\varepsilon(\omega) = \varepsilon_\infty \prod_{\nu=1}^{4}\left(\frac{\Omega_{L\nu}^2 - \omega^2}{\Omega_{T\nu}^2 - \omega^2}\right). \tag{45}$$

High-frequency permittivity ε_∞ is almost the same as $\varepsilon_{\mathrm{ele}}$. Refer to the original papers [47] and [48] for the detailed derivation process. Since $BaTiO_3$ includes five ions, there are 15 degrees of freedom, three among which are "acoustic," and 12 are "optical" modes. 1/3 of 12 are longitudinal, and the remaining 2/3, 8 are the transverse optical (TO) modes. Since the transverse modes are double-degenerated, we consider only four different "TO mode" eigenfrequencies in (45). In particular, taking into account low frequency or dc, $\omega = 0$ (i.e., low-frequency permittivity measurement!), we obtain

$$\frac{\varepsilon_S}{\varepsilon_\infty} = \prod_{\nu=1}^{4}\left(\frac{\Omega_{\mathrm{LO},\nu}^2}{\Omega_{\mathrm{TO},\nu}^2}\right). \tag{46}$$

This equation is known as the "Lyddane–Sachs–Teller (LST) relation" [49].

B. Soft Phonon Modes in Relaxor Ferroelectrics

We now discuss "softening" (i.e., eigenvibration frequency decrease as the effective spring constant decrease!) of phonon modes relating to the paraelectric–FE phase transition. Regarding the longitudinal modes, even if Ω_{LO} decreases to zero with approaching the Curie temperature T_C, the permittivity increase cannot be expected. This is obvious because the longitudinal wave maintains $D = 0$ even under electric field applied, leading to $\varepsilon_S = 0$ theoretically. Thus, to explain the divergence of permittivity (i.e., the Curie–Weiss law), we should consider the "TO" eigenfrequency $\Omega_{\mathrm{TO},\nu}$ decrease. The optical mode frequencies are generally higher than the acoustic modes around $k \approx 0$ if no interaction exists between each eigenmode. As well-known [50], [51], in a perfectly harmonic crystal, the phonon states are stationary, widespread in the crystal uniformly with a monotone frequency as a wave (that is, NOT an isolated wave packet or particle-like phonon). However, when the atomic energy potential includes a nonlinear term, "cubic" anharmonic term introduced in (28), or "quartic" term, the resonance frequency should include at least $2\omega_0$ or $3\omega_0$, higher order harmonic modes. According to the uncertainty of the resonance frequency from the definite $\omega = \omega_0$ to $\Delta\omega = |\omega - \omega_0|$, the phonon distribution changes from an infinitely widespread state in a crystal to a sort of wave-packet status (i.e., localized existence). This "anharmonicity" in the atomic potential is the key factor to create the phonon–phonon interaction in the crystal lattice and the "softening of the TO phonon mode." Kurosawa [48] indicated that this TO mode corresponds to the cations shift with respect to the oxygen octahedron without twisting, which corresponds to the tetragonal symmetry BT structure.

If we assume the descendent frequency of one of the "TO" modes linearly with temperature as

$$\left(\Omega_{\mathrm{TO}}^{\mathrm{soft}}\right)^2 = A(T - T_C) \tag{47}$$

we can derive the Curie–Weiss law from (47) [i.e., "critical slowing down"]. If we assume that the remaining mode frequencies (except for the above TO mode) are relatively insensitive to the composition and temperature, we can rewrite the LST relation as

$$1/\varepsilon_S = K'\left(\Omega_{\mathrm{TO}}^{\mathrm{soft}}\right)^2. \tag{48}$$

Thus, the Curie–Weiss constant C can be expressed as

$$C = 1/K'A. \tag{49}$$

On the other hand, adopting (14) and (16), the electrostrictive coefficient Q can be expressed in terms of soft phonon mode parameters, A and K'

$$\frac{\partial(1/\varepsilon_S)}{\partial p} = 2\varepsilon_0 Q_h [Q_h = Q_{11} + 2Q_{12}] \tag{50}$$

$$Q_h = \left[-\frac{1}{2}\frac{\partial(T_C)}{\partial p}\right] K' A. \tag{51}$$

If we accept the empirical rule that the $((\partial(T_C)/\partial p))$ value is roughly constant for all perovskite FEs reported by Samara [12], we can understand "$Q_h C$ = constant" rule based on the soft phonon model. The empirical rule "$((\partial(T_C)/\partial p))$ = constant" in perovskite FEs is again the key to be theoretically solved in the future. The soft phonon mode is typically observed by the "Raman spectroscopy" with a typical sweeping wavenumber range of 200–2000 cm^{-1} in normal FEs.

Disordered perovskites, such as $Pb(Mg_{1/3}Nb_{2/3})O_3$ and $Pb(Fe_{1/2}Ta_{1/2})O_3$, tend to be FE. In addition, the phase transition of the disordered perovskite is rather diffused, and the crystal structure in the low-temperature phase is rhomboidal, rather than tetragonal in $BaTiO_3$ and $PbTiO_3$. When giant electrostriction and enormous electromechanical coupling factor were discovered in these relaxor FEs in the early 1980s, no soft modes were observed in the Raman spectra of disordered complex perovskite FEs by Burns and Scott [52].

Thus, the possible wavenumber for the soft phonon modes in relaxor FEs was speculated in the frequency range below 20 cm^{-2} by Uchino *et al.* [53]. Assuming a Gaussian distribution of the local Curie temperature around the average $\langle T_C \rangle$, as proposed by Rolov [54]

$$\left[\Omega_{\mathrm{TO}}^{\mathrm{soft}}(T)\right]^2 = \frac{\int_0^T A(T - T_C)\exp\left[-\frac{(T_C - T_{\mathrm{av}})^2}{2\delta^2}\right] dT_C}{\int_0^\infty \exp\left[-\frac{(T_C - T_{\mathrm{av}})^2}{2\delta^2}\right] dT_C} \tag{52}$$

the soft phonon frequency was simulated [refer to Section VII-B]. Here, T_C is a local Curie temperature, $T_{\mathrm{av}} = \langle T_C \rangle$ taken as the 1 kHz (low frequency) permittivity peak temperature, where it is suggested that some 50% of the specimen has passed into the FE form, and δ is a parameter describing the diffuseness of the phase transition. $\Omega_{\mathrm{TO}}^{\mathrm{soft}}$ for $Pb(Mg_{1/3}Nb_{2/3})O_3$ single crystals was predicted with A = 3.4 $cm^{-2}K^{-1}$ and δ = 41 K as a small but finite value of $\Omega_{\mathrm{TO}}^{\mathrm{soft}} \sim 7$ cm^{-1} at $T = T_{\mathrm{av}}$ [53]. Note almost an order-of-magnitude lower A constant compared with that in $SrTiO_3$, $KTaO_3$ [55], and $PbTiO_3$ [56].

Since then, the Raman spectroscopy has been improved continuously by various researchers, such as Al-Zein *et al.* [57], Taniguchi *et al.* [58], and Hehlen *et al.* [59] for observing the soft modes below 20 cm^{-1} in relaxor FEs. The above prediction was confirmed during this period with precise light scattering studies. Kojima's group developed a "broadband micro-Brillouin scattering spectroscopy" by combining an optical microscope and the Fabry–Perot interferometer, with the capabilities of a spatial resolution of a few mm in the low-frequency (GHz) window between 0.03 and 33 cm^{-1} [60]. This equipment could observe a specific softening of both optical and acoustic modes in PMN-PT and PZN-PT crystals down to 1 cm^{-1}. Peculiar acoustic anomalies in PMN-35%PT were reported [61]: longitudinal acoustic (LA) mode frequency showed a substantial softening around 1.5 cm^{-1} upon cooling toward the T_C under assumptions that dynamical behaviors of PNRs should be observed as quasi-elastic scattering (or "central peak") in inelastic scattering experiments in a 0.03–33-cm^{-1} range, and the polarization fluctuations of PNRs are coupled to acoustic phonons [60]. The 1-cm^{-1} region dynamics in PMN-PT and PZN-PT clarified the precursor dynamics of PNRs, associated with the TO mode softening. The formation and growth of PNRs provide substantial effects on the acoustic modes due to the "electrostrictive coupling" between them even in the paraelectric region. Softening of both LA and TA modes, as well as their increasing attenuations, has commonly been observed in both PMN-PT and PZN-PT relaxors. Furthermore, these acoustic anomalies were accompanied by the appearance of quasi-elastic central peaks that reflect polarization reorientation processes of dynamic PNRs. This "polar nanoregion model" seems to be directly related to the discussions in Sections VII and VIII. The "soft vibration mode" has not clearly been discussed yet, which stabilizes a rhombohedral (rather than tetragonal) crystal symmetry of the perovskite structure.

It would also be intriguing to study the lattice vibration mode softening in ordered and disordered crystals with the same composition, in which the degree of order is controlled by annealing, such as $Pb(Sc_{1/2}Ta_{1/2})O_3$ [28]. Higher soft mode frequency, in addition to higher Curie temperatures T_C and electrostrictive coefficients Q, is expected with increasing the degree of order. The theoretical analysis with a precise physical model is expected in this anharmonic vibration treatment.

VII. Critical Exponent in Relaxor Ferroelectrics

A. Dielectric Relaxation

One of the significant characteristics of these "relaxor FEs" is "dielectric relaxation" (i.e., the frequency dependence of the permittivity), from which their name is derived. The temperature dependence of the permittivity and dielectric loss for $Pb(Mg_{1/3}Nb_{2/3})O_3$ is shown in Fig. 9(A) at various measuring frequencies by Smolensky *et al.* [62]. With increasing the measuring frequency, the permittivity in the low-temperature (FE) phase decreases, and the peak temperature near 0 °C shifts toward higher temperature; this is contrasted with the behavior of normal FEs, such as $BaTiO_3$, where the peak temperature changes little with the frequency. It should also be pointed out that the permittivity ε in the paraelectric phase does not follow the famous Curie–Weiss law though dielectric dispersion is not significant, while dielectric loss shows large dispersion in the paraelectric phase.

The dielectric relaxation apparently similar to the above-mentioned $Pb(Mg_{1/3}Nb_{2/3})O_3$ can be observed also in NP disordered perovskites. Fig. 9(B)(a) shows the permittivity (real and imaginary parts) versus temperature curves of the $(K_{3/4}Bi_{1/4})(Zn_{1/6}Nb_{5/6})O_3$ single crystal [63]. The permittivity peak is not associated with the phase transition, and the

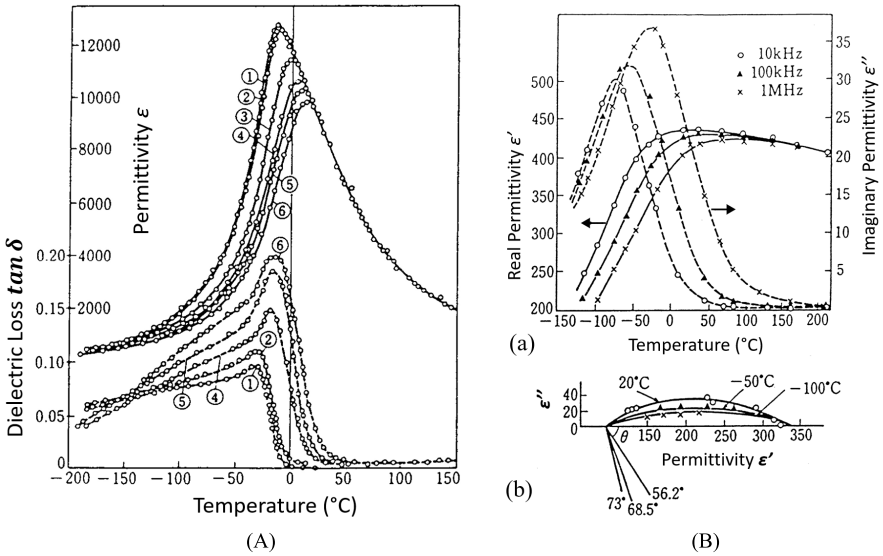

Fig. 9. (A) Temperature dependence of the permittivity and loss tanδ in $Pb(Mg_{1/3}Nb_{2/3})O_3$ for various measuring frequencies (kHz): (1) 0.4; (2) 1; (3) 45; (4) 450; (5) 1500; and (6) 4500 [62]. (B) (a) Permittivity versus temperature curves of the $(K_{3/4}Bi_{1/4})(Zn_{1/6}Nb_{5/6})O_3$ single crystal. (b) Cole–Cole plot [63].

cubic crystal structure is maintained through the measuring temperature range. When a Cole–Cole plot of the real and imaginary parts of the permittivity is drawn [see Fig. 9(B)(b)], multidispersive characteristics can be observed especially in a low-temperature range. As well known, when we consider a double-potential-well "Debye" model, we obtain a Debye dispersion relation [38]

$$\varepsilon^*(\omega) - \varepsilon_0 = (\varepsilon_\infty - \varepsilon_0)/(1 + j\omega\tau) \tag{53}$$

which traces a half-circle. To the contrary, the shallow arc shape dispersion in Fig. 10(B)(b) can be expressed by

$$\varepsilon^*(\omega) - \varepsilon_0 = (\varepsilon_\infty - \varepsilon_0)/\left[1 + (j\omega\tau)^\beta\right] \tag{54}$$

where $\beta < 1$. This is caused by shallow multipotential wells in a locally distorted perovskite cell due to the disordered ionic arrangement ("Skanavi-type dielectric relaxation") [64]. The Skanavi-type provides local dipoles and exhibits an "electret"-like property. Of course, when no electric field is applied initially, no charge or polarization is expected because of no cooperative coupling in the crystal. One of the possible conventional explanations for the "dielectric relaxation" of the "relaxor FEs" is to couple this Skanavi-type relaxation with the long-range "dipole coupling" for revealing the net spontaneous polarization and ferroelectricity. However, Viehland *et al.* [65] and Krause *et al.* [71] proposed another possibility in terms of the interaction among microdomains in Section VIII-C.

B. Classic Diffuse Phase Transition Model

Another significant characteristic of relaxor FEs is its "diffuse ("smeared" was used previously) phase transition," the reason for which has not yet been clarified. We introduce here a classic "microscopic composition fluctuation" model widely accepted model for the relaxor FEs [66]–[70]. A single "Känzig region," the minimum polar region size in which cooperative polarization (ferroelectricity) can occur, has typically on the order of 10–100 nm [70], which is recently called "PNR." Krause *et al.* [71] have reported the short-range ionic ordering of $Pb(Mg_{1/3}Nb_{2/3})O_3$ observed by electron microscopy. The high-resolution electron-microscope image revealed somewhat ordered islands in the range of 2–5 nm in the disordered sea, each of which may have a slightly different transition temperature.

Because of a rather broad permittivity peak, sometimes, the "Curie temperature range" is specified rather than the "Curie point." Rolov [54] assumed that physical properties in a local Känzig region may not change drastically due to the composition (x) fluctuation, but that only the local Curie temperature T_C should be changed in proportion to the composition fluctuation Δx $(= x - x_{\text{av}})$, namely,

$$r = (T_C - T_{\text{av}})/(x - x_{\text{av}}) \tag{55}$$

where T_{av} is an average Curie temperature and r is a constant. Then, the distribution of the local Curie temperature was introduced by

$$f(T_C) = \left(1/\sqrt{2\pi\sigma^2}\right)\exp\left[-(T_C - T_{\text{av}})^2/2\sigma^2\right] \tag{56}$$

where σ is the standard deviation of this Gaussian type. Note that the Gaussian distribution is based on no interaction among each Känzig cluster ("nanopolar region"). Based on this statistical distribution of the Curie temperature and the FE phenomenology, physical properties can be estimated theoretically. If the fluctuation of the local composition (not a mesoscopic compositional inhomogeneity!) is large enough to provide $\sigma \gg 10$ °C, the normal Curie–Weiss law for each microregion

$$1/\varepsilon = (T - T_0)/C \,(T_0 : \text{Curie–Weiss temperature}) \tag{57}$$

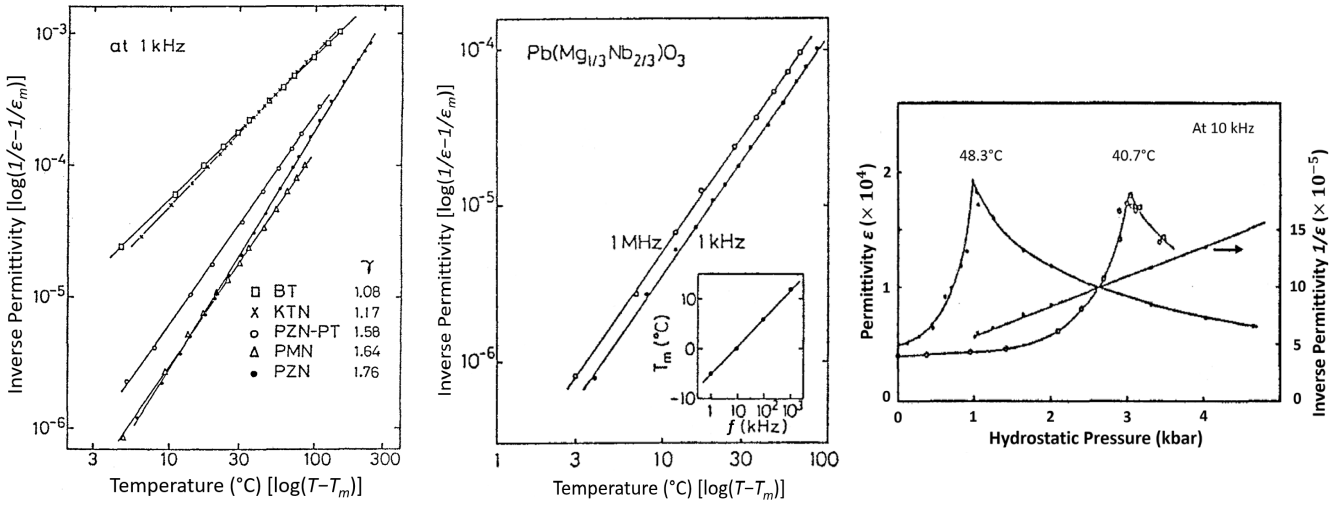

Fig. 10. (a) Logarithmic plots of the reciprocal permittivity $(1/\varepsilon - 1/\varepsilon_m)$ at 1 kHz versus temperature $(T - T_m)$ relation for $BaTiO_3$ (BT), $K(Ta_{0.55}Nb_{0.45})O_3$ (KTN), $0.88Pb(Zn_{1/3}Nb_{2/3})O_3$-$0.12PbTiO_3$ (0.88PZN-0.12PT), $Pb(Mg_{1/3}Nb_{2/3})O_3$ (PMN), and $Pb(Zn_{1/3}Nb_{2/3})O_3$ (PZN). The γ values were determined in the temperature range of 5 °C $< T - T_m <$ 200 °C. (b) Frequency dependence of the critical exponent γ for PMN [72]. (c) Permittivity ε and inverse permittivity $1/\varepsilon$ at 10 kHz versus hydrostatic pressure p relation for $K(Ta_{0.55}Nb_{0.45})O_3$ (KTN) [72].

is transformed into

$$1/\varepsilon = (1/\varepsilon_m)\exp\left[-(T - T_{\text{av}})^2/2\sigma^2\right] = (1/\varepsilon_m)\left[1 + (T - T_{\text{av}})^2/2\sigma^2 + (T - T_{\text{av}})^4/8\sigma^2 + \cdots\right] \tag{58}$$

where ε_m is the maximum permittivity at $T = T_{\text{av}}$. Taking the first approximation, (58) provides a following "square" rule in the diffused phase transition by neglecting higher order terms of the Taylor expansion series:

$$(1/\varepsilon - 1/\varepsilon_m) \propto (T - T_m)^2. \tag{59}$$

However, Uchino and Nomura [72] pointed out discrepancies in the inverse permittivity curve fitting to either linear $(T - T_m)$ or quadratic $(T - T_m)^2$ and convex or concave curves, respectively, just above the permittivity peak temperature $(T - T_m < 30$ °C), which may be related to the Gaussian distribution assumption without considering the "microdomain–microdomain interaction." This motivated the critical exponent with a fractal model later.

C. Introduction to Critical Exponent

Uchino and Nomura [72] proposed the "critical exponent" γ in the relation between the dielectric constant and temperature (or hydrostatic pressure). A high correlation of the γ value with the phase transition diffuseness was found empirically. Though this formula has initially been introduced just as an "empirical curve fitting," it leads to the fractal analysis approach 20 years after, by taking into account the mesoscopic domain–domain interaction around the phase transition range. Refer to Section VIII. The critical exponent γ was introduced in a form

$$(1/\varepsilon - 1/\varepsilon_m) = C'^{-1}(T - T_m)^{\gamma} \tag{60a}$$

not only for relaxor FEs but also for normal sharp-transition FEs so that (60a) may provide the best fit to the experimental results in a wide temperature range. Moreover, another critical exponent γ^* of the permittivity with respect to hydrostatic pressure p, which is given by

$$(1/\varepsilon - 1/\varepsilon_m) = C^{*-1}(p - p_m)^{\gamma *} \tag{60b}$$

has also been determined for the same specimens.

1) Temperature Dependence of Permittivity: Temperature dependence of permittivity was measured in single crystals of $Pb(Mg_{1/3}Nb_{2/3})O_3$ (PMN) and $Pb(Zn_{1/3}Nb_{2/3})O_3$ (PZN) with a very diffused phase transition, $BaTiO_3$ (BT) and $K(Ta_{0.55}Nb_{0.45})O_3$ (KTN) with a sharp phase transition, and a solid solution crystal $0.88Pb(Zn_{1/3}Nb_{2/3})O_3$-$0.12PbTiO_3$ (0.88PZN-0.12PT). Fig. 10(a) shows logarithmic plots of the reciprocal permittivity $(1/\varepsilon - 1/\varepsilon_m)$ measured at 1 kHz as a function of temperature $(T - T_m)$. The linearity of the curves is remarkably good except in a very narrow temperature range above the peak T_m $(T - T_m < 1$ °C) for all the specimens. The critical exponent γ of the reciprocal permittivity with respect to temperature has been determined from the slope of the straight line in the range of 5 °C $< T - T_m <$ 200 °C: $\gamma = 1.08$ for BT, 1.17 for KTN, 1.58 for 0.88PZN-0.12PT, 1.64 for PMN, and 1.76 for PZN. Note that this γ is different from the conventional "critical exponent" defined for sharp-transition FEs, such as BT in very close vicinity of the Curie temperature $(T - T_C < 1$ °C). Table II summarizes the critical exponent γ and the Curie-like constant C' for all the specimens in the first and second columns. It is important to mention here that the relaxor FEs reveal a large relaxation of the permittivity and also that the exponent γ might be changed with measuring frequency. PMN, for example, shows a gradual decrease in the permittivity ε and a monotonous increase in the peak temperature T_m with changing the measuring frequency from 1 kHz to 1 MHz, as inserted in Fig. 10(b). The critical exponent γ (i.e., line slope) seems to be insensitive to the frequency change at least in the range below 10 MHz, while the constant C' (i.e., the bias of the line) varies with the

TABLE II
CRITICAL EXPONENTS OF THE PERMITTIVITIES γ AND γ^*, AND THE CURIE-LIKE CONSTANT C' FOR RELAXOR AND NORMAL-TRANSITION FEs

Substances	γ	C' (x10^5)	γ^*
$BaTiO_3$	1.08	2.1	1.0[a)]
$K(Ta_{0.55}Nb_{0.45})O_3$	1.17	2.9	1.00
$0.88Pb(Zn_{1/3}Nb_{2/3})O_3$-$0.12PbTiO_3$	1.58	63	–
$Pb(Mg_{1/3}Nb_{2/3})O_3$	1.64	140	1.66
$Pb(Zn_{1/3}Nb_{2/3})O_3$	1.76	200	–

a) Reference [74]

frequency. Though the application of the Vogel–Fulcher law derives the nonlinear relation between the peak temperature T_m and $\log(f)$ [73], the inserted result in Fig. 10(b) seems to be rather straight.

2) Pressure Dependence of Permittivity: The effect of hydrostatic pressure on the dielectric constant was also investigated for PMN, KTN, and BT single crystals [72], [74]. A new critical exponent γ^* of the permittivity with respect to pressure was introduced by the definition of (60b). Fig. 10(c) shows the data for KTN: 10-kHz permittivity ε and inverse permittivity $(1/\varepsilon)$ as a function of hydrostatic pressure p for two different temperatures, where the maximum permittivity pressure is denoted as p_m, which corresponds to the phase transition pressure (equivalent to T_C in the temperature plot) [72]. Logarithmic plots of the reciprocal permittivity $(1/\varepsilon - 1/\varepsilon_m)$ at 10 kHz versus pressure $(p - p_m)$ relation provide the slope (exponent γ^*): $\gamma^* = 1.00$ for KTN and 1.66 for PMN. The critical γ^* exponents are also summarized in Table II, including the value for BT reported by Samara [74]. It is important to note that the critical exponent γ^* of the permittivity with respect to hydrostatic pressure is rather close to the γ value in both the relaxor and normal FEs.

This correspondence was consistently explained by assuming that the reciprocal dielectric constant is represented by the following general formula:

$$(1/\varepsilon - 1/\varepsilon_m) = C'^{-1}(T - T_m - [\partial T_m(p)/\partial p] \cdot p)^{\gamma}. \quad (61)$$

The transformation of (61)

$$1/\varepsilon - 1/\varepsilon_m = C'^{-1}|\partial T_m(p)/\partial p|^{\gamma}(p - (T - T_m)/[\partial T_m(p)/\partial p])^{\gamma} \quad (62)$$

gives the relations of

$$\gamma^* = \gamma \quad (63a)$$

$$C^* = C'|\partial T_m(p)/\partial p|^{-\gamma}. \quad (63b)$$

3) Critical Exponent Discussion: It is worth noting the correlation between the critical exponent γ and the phase transition diffuseness. Refer to Table II. BT revealing a typical sharp phase transition has a γ value nearly equal to 1: this corresponds to the Curie–Weiss law. The solid solution KTN with an "apparent" sharp transition reveals a slight deviation from the Curie–Weiss law. However, as demonstrated in Fig. 8(b), this solid solution exhibits a bit wider polarization fluctuation range, which gives $\gamma = 1.17$. This may be the reason why we could observe the enhanced electrostrictive coefficient Q^{obs} in a relatively wide (~20 °) temperature range. On the other hand, the γ value is as large as 1.7 for PMN and PZN with a very diffused transition; however, this is relatively smaller than the expected "2" for the "quadratic law" proposed by Smolenskii [75]. The solid solution PZN-PT between a relaxor and a normal-transition FEs reveals an intermediate γ value of 1.58. The critical exponent γ of the permittivity, determined in the temperature range from several to several hundreds of °C above the transition point, may at least represent the degree of the phase transition diffuseness.

VIII. FRACTAL ANALYSIS OF DOMAIN CONFIGURATIONS IN FERROELECTRICS

As demonstrated in "ice" crystal structure (i.e., "hexagonal" snowflake), physical performance in a large crystal may be governed by semimicroscopic configuration with increasing the crystal size. "Fractal analysis" is used to discuss the intermediate between macroscopic phenomenology in infinitely large uniform material in Section II and the microscopic atomic/lattice viewpoint discussed in Section IV. Let us consider the origin of "self-similarity" of hexagonal snowflake configurations, for example. When a new cluster (i.e., water particle) approaches an existing snowflake, it can be deposited easily at the tip of the branch, while it may be difficult to reach into the joint part. This intuitive model can explain that the snow crystal grows with keeping the original sixfold symmetry shape. The key is to consider the cluster (new-comer)–cluster (ready-existing) interaction. Because FEs (relaxor FEs, in particular) generate a macroscopic domain pattern with decreasing temperature (i.e., growth of PNRs) through its phase transition temperature range originated from micro–micro-domain interaction from an elevated temperature, similar fractal behavior can be anticipated.

A. Domain Configuration and Dielectric Relaxation

Viehland *et al.* [33] investigated the polarization behavior of La-modified lead–zirconate–titanate (PLZT) relaxors for various electrical and thermal histories. The field-cooled and zero-field-cooled behaviors were both studied. The magnitude of both polarizations was found to be equal above a critical temperature. A macroscopic polarization is developed when the zero-field-cooled state was warmed with a bias applied. The origin of the "dielectric relaxation" from the microdomain state was demonstrated in $Pb(Zn_{1/3}Nb_{2/3})O_3$ single crystals by Mulvihill *et al.* [76]. Fig. 11(a) and (c) shows the dielectric

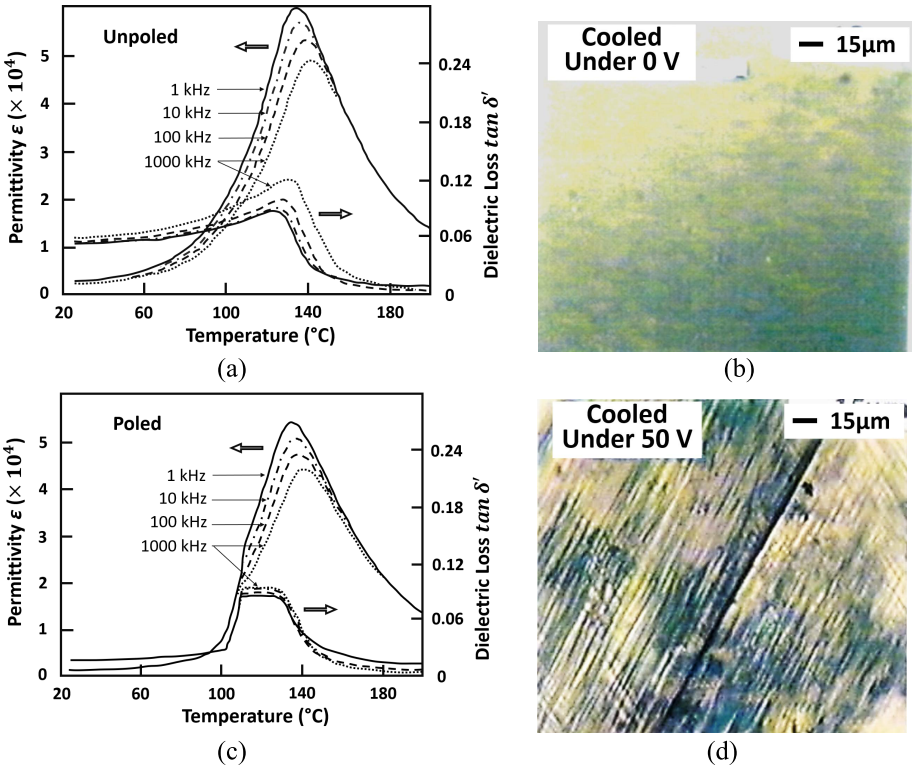

Fig. 11. Dielectric constant and loss versus temperature measured for $Pb(Zn_{1/3}Nb_{2/3})O_3$ single crystals on the [111] plates: (a) unpoled state and (c) poled state. The domain configurations are also pictured in (b) and (d) [77].

constant and loss versus temperature for 1–1000 kHz on an unpoled and a poled PZN single crystal [111] plate specimen, respectively (electric field along the spontaneous polarization direction ⟨111⟩), where the poled specimen shows smaller permittivity and loss tan δ' due to lower permittivity along P_S. The domain configurations are also pictured in Fig. 11(b) and (d). The macroscopic domains were not observed in an unpoled sample even at room temperature, only in that state large dielectric relaxation and loss were observed below the Curie temperature range. Once the macrodomains were induced by an external electric field [notice spindle-like domains (2–3 μm width) in Fig. 11(d)], the dielectric dispersion disappeared, and the loss became very small (that is, the dielectric behavior became rather normal!) below 105 °C. As the temperature is increased, the macroscopic spindle-like domains disappear suddenly in the poled specimen at 105 °C [i.e., a sort of the macro–micro-domain configuration transition temperature], and then, immediately above this temperature, both large dielectric dispersion and loss appear [see Fig. 11(c)]. Thus, we can conclude the following.

1) The dielectric relaxation phenomenon and associated high dielectric loss tan δ' in the unpoled PZN seem to be originated from the microdomain dynamics. Due to a slow micro-domain–domain interaction, dielectric response delay may happen. This argument is consistent with the lattice mode softening originated from the "PNR dynamics" indicated by Kojima and Ko [61].
2) There seems to exist a sort of transition, macro-to-micro-domain sudden change, around 105 °C in PZN. It is intriguing that the macrodomain will not gradually diminish.

When the PMN single crystal was poled, the macroscopic domain pattern was observed at very low temperature of −196 °C [Private communication with Mulvihill (1996)].

How we can reconcile the previous Skanavi multipotential model and this microdomain interaction model for the dielectric relaxation is still not clear. The author also anticipates the construction of the macro-to-micro-domain transition theory (not a gradual continuous domain size change).

B. Fractal Analysis of Ferroelectrics

The critical exponent $1 < \gamma < 2$ of the extended hyperbolic relation $1/\varepsilon \propto (T - T_m)^{\gamma}$ suggests a fractal behavior of these FE materials in terms of temperature (and pressure), which may be originated from the microdomain–microdomain interaction, as demonstrated in Fig. 11. The Cole–Cole dispersion of the relaxor expressed as $\varepsilon^*(\omega) = \varepsilon_\infty/[1 + (j\omega\tau)^{\beta}]$ with $\beta < 1$ comes basically from the same origin, where the fractal behavior is observed in terms of time/frequency (i.e., with a parameter τ, damping constant/life time). Micro-to-macro FE domain growth changes the domain dynamics, leading to changes in various physical properties, such as dielectric permittivity, loss, polarization hysteresis, and acoustic emission (AE). The following discussion is based on [77] and [78].

1) Fractal Analysis of the Electric-Field-Induced AE:

a) Definition of fractal dimension: When the "self-similarity" of the cluster shape can be maintained by reducing the geometrical scale, the "fractal dimension" is defined as

follows. There are N particles with each radius r_i, which makes a cluster. The average cluster radius R can be estimated in the 2-D case by

$$R = \left(\sum_i^N \frac{r_i^2}{N} \right)^{1/2}. \tag{64}$$

If the number of particles N is related to R as

$$N \sim R^D. \tag{65}$$

D is called the "fractal dimension." Like a snowflake in the 2-D, if the clusters do not have interaction with each other, the circle (πr^2) is filled by clusters fully, leading to $D = 2$. Because of the cluster–cluster interaction between water particles (i.e., rejecting some clusters to fill in around the branch joint), the snowflake pattern results in $0 < D < 2$ (i.e., smaller N). The fractal dimension provides a "shape pattern" information. It is also not difficult for the reader to extensively imagine that $D = 1$ for a string and $D = 3$ for a sphere configuration.

Supposing that a "contour shape" is a function $f(r)$ and "scaling parameter" is λ, in order to maintain the contour shape, the function $f(r)$ should keep

$$f(\lambda r) = g(\lambda)^* f(r). \tag{66}$$

This is known as "scaling law." We obtain a relationship for the "scaling function" $g(\lambda)$

$$g(\lambda\mu) = g(\lambda)^* g(\mu) \tag{67}$$

leading to the power law for the scaling function $g(\lambda)$

$$g(\lambda) = \lambda^p \tag{68}$$

where p can be "noninteger."

Uchino [78] translated (68) in relaxor FEs as follows. The "Känzig" or "polar nanoregion" corresponds to a "cluster," which has the Curie temperature T_C distribution ($T_C - T_{\text{av}}$) due to the composition (or position) fluctuation ($x - x_{\text{av}}$). If we assume that $(T_C - T_{\text{av}})/(x - x_{\text{av}}) =$ constant, we can take $(T - T_{\text{av}})$ as a scaling parameter λ. Based on the local Curie–Weiss law $(1/\varepsilon - 1/\varepsilon_m) \propto (T - T_m)$ in each cluster, the scaling function corresponds to the inverse permittivity, and then, the following critical exponent equation is expected:

$$(1/\varepsilon - 1/\varepsilon_{\max}) \propto (T - T_{\text{av}})^p \tag{69}$$

where p is noninteger, which corresponds to the "critical exponent" discussed in Section VII.

It is noteworthy here that the Gaussian distribution model by Rolov [54] and the well-accepted Vogel–Fulcher model consider the probability of polar nonoregions in terms of energy/temperature without considering the micro-cluster–cluster interaction explicitly (that is, the fractal dimension seems to be 3), which is contradictory to the fractal dimension reported in relaxor FEs [72] described in Section VIII-B2.

b) Fractal dimension in acoustic emission: The AE method is a nondestructive technique used to detect pulses of released elastic strain energy caused by deformation, crack growth and phase change, and domain motions in ferromagnetic and FE materials. A fractal analysis of the AE signal amplitude distribution, which is used in the AE method to determine the damage configurations of materials originally by Nakase [79], was also adopted by Aburatani *et al.* [77] for the FEs though no damage. When the AE event rate $f(x)$ is the minus Dth power of x, where x is the AE signal amplitude

$$f(x) = cx^{-D} (c\text{: constant}) \tag{70}$$

the number of D is supposed to be defined as the fractal dimension. The integrated AE event $F(x)$

$$F(x) = \int_x^\infty f(x) \cdot dx = \frac{1}{D-1} cx^{-D+1} (D > 1) \tag{71a}$$

is observed through changing the AE signal threshold level in the measurements. If $D = 1$,

$$F(x) = \int_x^\infty f(x) \cdot dx = c \ln x + A. \tag{71b}$$

c) Electric-field-induced AE: Fig. 12(a) shows the AE event count rate and the induced displacement of the FE PZT ceramic disk as a function of the applied field at 0.0015 Hz with field levels of ±35 kV/cm [77]. During an electric field cycle showing a butterfly-shaped displacement curve, no AE was observed from zero to the coercive field at which the induced displacement took a minimum. The critical electric field, where the AE started to be generated, was slightly higher than the coercive field. This critical electric field corresponded to the point of inflection at which the second derivative of the displacement with respect to the field, that is $\partial^2(\text{displacement})/\partial E^2$, changes the sign. Since the displacement induction rate started to decrease in spite of the field simply increasing and the AE was present above this field, these results might indicate that a damping process for the sample deformation existed above this field, and the AE was generated through that process. It is worth noting that the maximum event rate occurred at around 27.5 kV/cm. Considering that the internal stress increases with the applied field in FEs, if this observed AE was caused only by the internal stress, the AE event count rate should have increased with the applied field. Thus, this decrease in the AE event rate might suggest that the internal stress could be the origin of the AE but not only one source. Since the induced displacement in the FE ceramics consists of the "domain reorientation" related to deformation and "piezoelectric deformation" without the domain reorientation, it was assumed that the field-induced AE in the PZT ceramics was generated first through domain reorientation related deformation, and after domain reorientation was completed, the piezoelectric deformation (unrelated to domain reorientation), which was accompanied with induced stress, was expected to be the origin of the AE. The decrease in the AE event might indicate the completion of the domain reorientation-related deformation. Note that the AE is observed only when the displacement is increased, and no AE appears during the displacement decrease process [i.e., known as the "Kaiser effect"].

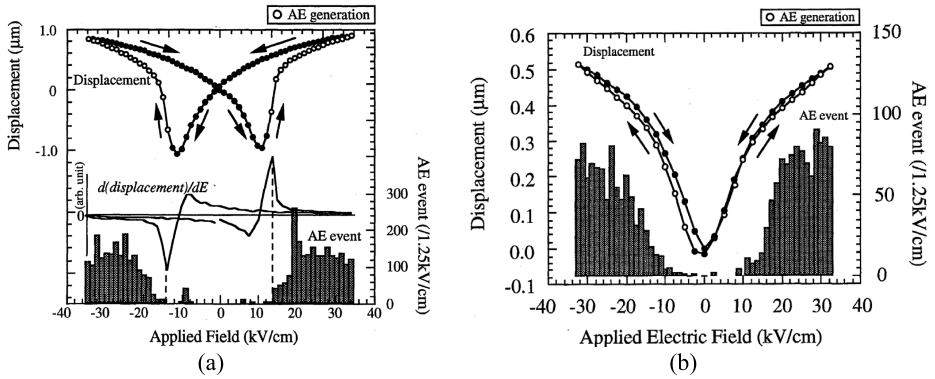

Fig. 12. AE event count and the induced displacement as a function of the applied electric field in (a) FE PZT and (b) electrostrictive 0.9 PMN-0.1 PT [78].

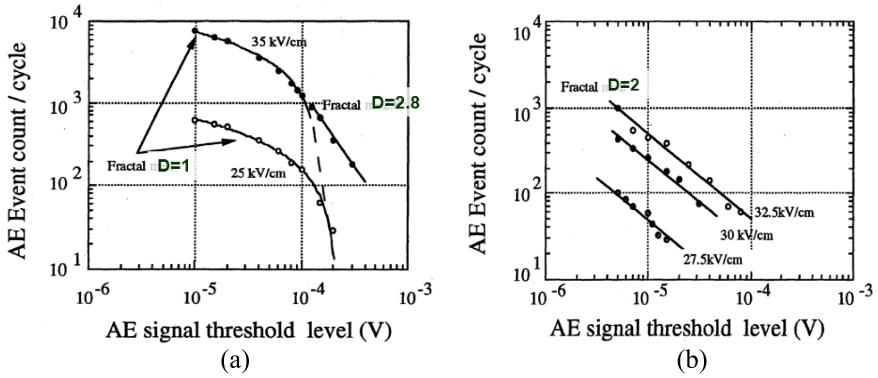

Fig. 13. AE event count per cycle as a function of the AE signal threshold level: (a) FE PZT and (b) electrostrictive 0.9 PMN-0.1 PT.

To the contrary, Fig. 12(b) shows the induced displacement and AE event count rate in the electrostrictive 0.9PMN-0.1PT ceramics. A quadratic induced displacement, which showed much less hysteresis than that of FE PZT ceramics, was observed. The AE count rate increased with the applied field. Because of the absence of the large domain in PMN-PT, the induced displacement might not be caused by the macroscopic domain reorientation but "electrostrictive deformation" (maybe "microdomain growth process"). It was assumed that the origin of the AE was the internal stress caused by the electrostrictive deformation, resulting in the increased AE event rate in proportion to the electrostriction with the applied electric field.

The AE event count rate and the induced displacement in the "soft piezoelectric" PLZT(9/65/35) ceramics (see data in [77]) are very suggestive. A sharp peak of the AE event rate was first observed around 10 kV/cm, and the AE event rate again increased with the applied field in proportion to the induced displacement when a field was higher than 10 kV/cm. The first peak of the AE event rate was due to the domain reorientation-related deformation, and after the domain reorientation was completed, the AE was caused by the piezoelectric deformation (unrelated to domain reorientation).

2) Discussion on the Fractal Dimension:

a) PZT: Fig. 13(a) shows the AE event count per cycle as a function of the AE signal threshold level (log–log plot) in the FE PZT ceramics. The observed AE event count logarithmically decreases with the AE signal threshold level when a field of ±25 kV/cm is applied. Thus, a fractal dimension of $D = 1$ can be obtained for the logarithmic decrease in the FE PZT. Since repeatable and stable field-induced AE is observed, it is supposed that the lowered fractal dimension is due to the existence of FE domain and the effect of the domain reorientation-related deformation. When a field of ±35 kV/cm is applied, the higher AE signal threshold level parts do not follow the logarithmic curve. The lower signal threshold level region still could be fitted to a logarithmic curve, and the extended line also ends around the AE signal threshold level obtained for ±25 kV/cm. The fractal dimension of the higher signal threshold level part can be found to be $D = 2.8$. Since the domain reorientation is supposed to be completed at a higher electric field, the origin of the AE with the fractal dimension of 2.8 is assumed to be piezoelectric deformation without domain reorientation. It is noted that the fractal dimension of the field-induced AE for the domain reorientation-related deformation ($D = 1$) is lower than that for the piezoelectric deformation without domain reorientation ($D = 2.8$).

b) PMN-PT: Fig. 13(b) shows the AE event count for the electrostrictive PMN-PT versus the AE signal threshold level. The same slopes for the AE event count are observed at various applied fields, and the critical fractal dimension of $D = 2$ can be obtained. It seems that the origin of AE in the electrostrictive PMN-PT ceramics does not change with the applied field level; thus, it is assumed to be originated from the internal stress caused by the electrostrictive deformation or microdomain/nanodomain growth/ dynamics. It is obvious

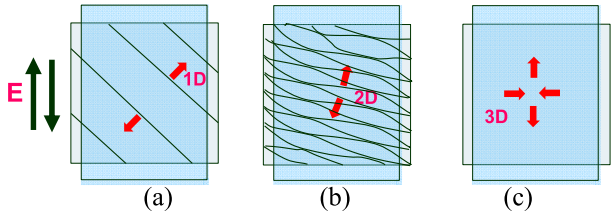

Fig. 14. Intuitive domain dynamics models: (a) macrodomain reorientation, (b) microdomain/nanodomain motion, and (c) piezostriction in a monodomain state.

that, since the fractal dimension $D = 2$ cannot be explained by the statistical isotropic models ($D = 3$), such as the Gaussian model or the Vogel–Fulcher model, we need to integrate the microdomain–microdomain (or PNRs) interaction explicitly.

c) Comparison and consideration of the fractal dimension: In conclusion from the AE measurements, the fractal dimension of the normal FE PZT ceramics consists of the domain reorientation related $D = 1$ and the piezostriction related $D = 2.8$ when a high electric field cycle is applied. The fractal dimension of $D = 2$ was obtained for the electrostrictive PMN-PT (i.e., relaxor FEs). The fluctuation of the fractal dimension of 1.4–1.9 was observed depending on the applied electric field in PLZT (9/65/35) ceramics, which shows an intermediate state between PZT and PMN-PT in terms of the induced displacement [77].

The fractal dimensions in PLZT and PMN determined by light scattering experiments were reported as 1.7 and 2.4, respectively, by Shur *et al.* [80] and Koreeda [81]. Note that Koreeda's result on PMN was obtained from an unpoled sample with microdomains, while Aburatani *et al.*'s data [77] from AE were from the PMN-PT under a large electric field applied condition (i.e., PNR growth process). However, the fractal dimension of the relaxor type seems to be around 2. When we recall that the large domain wall moves in 1-D like a sideward spreading mode in PZT, and the spindle-like narrow domain behaves with a breathing mode (2-D expansion by keeping the length almost constant) in PZN [refer to Fig. 11(b)], we can understand the above fractal dimensions observed, while the saturated domain status (equivalent to a single domain) deformation (extension along three axes and shrinkage along one and two axes) under such a large field, leading to a large fractal dimension close to 3. Thus, an intuitive domain dynamics model was proposed by Uchino [78] in Fig. 14 for explaining the fractal dimension. Fig. 14(a) depicts macrodomain reorientation in PZT under a low electric field. Clear plate-like 90°-domain walls move primarily perpendicular to the plate (1-D motion). If the AE comes from this motion, that is, domain embryos accumulate only 1 dimensionally, the fractal dimension $D = 1$ can be explained. However, when the electric field is larger than the coercive field in PZT, the monodomain-like state will be realized. The deformation beyond this field level is caused by intrinsic piezoelectricity (elastic deformation), that is, 3-D deformation [1-D extension associated with 2-D shrinkage in Fig. 14(c)]. This suggests the fractal dimension $D = 2.8$, close to the lattice dimension 3. On the contrary, in PMN-PT, supposing

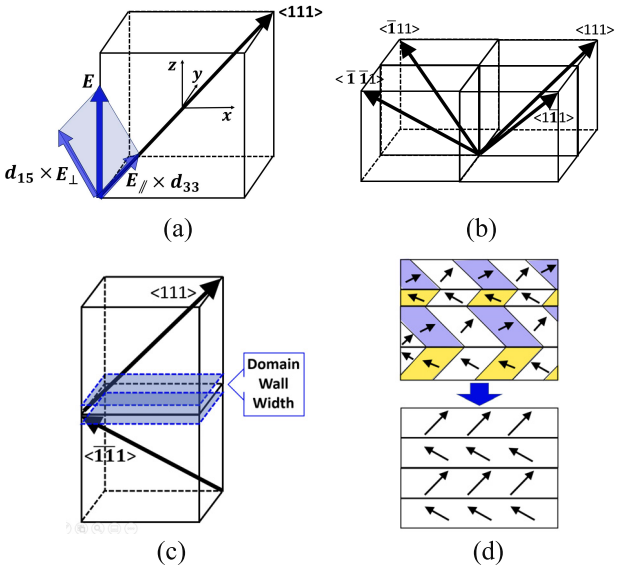

Fig. 15. Domain contribution transition: (a) monodomain state, (b) equal volumetric distribution of four domain states, (c) domain wall contribution model, and (d) macrodomain growth.

that the spindle-like microdomains breathe (i.e., fatter and slimmer like a rubber tube) under the electric field by keeping the length (i.e., PNR growth), as shown in Fig. 14(b), we can imagine $D = 2$ from this microdomain dynamics. Note again that we described the PMN-PT giant field-induced deformation as "electrostriction." However, it is not purely secondary-effect electrostriction (i.e., lattice anharmonicity) but a microdomain breathing/fatting phenomenon by combining multiple PNRs without significant visible hysteresis. Note that the "fractal dimension" determined by the AE seems to indicate the "PNR growth" configuration and the micro–micro-domain interaction. Further investigation of the domain dynamics is required for establishing a fractal model for the relaxor FE. As was derived the relationship between the critical exponent γ defined by the permeability $\chi \propto (T - T_C)^{-\gamma}$ and the fractal dimension in the Ising model in the ferromagnetic materials [82], the relationship between the critical exponent γ of permittivity and the fractal D is to be derived in FEs more explicitly in the near future.

IX. Domain Engineering

Because many of the recent fundamental researches are primarily focused on the improvement of electromechanical coupling performance in PZN-PT, PMN-PT single crystals, the author briefly summarizes them in this section. The key technology, "domain engineering," is composed of: 1) crystal orientation dependence of the physical performance; 2) domain size effect on the performance; and 3) poling techniques to generate the micro-to-macro-domain configuration.

A. Crystal Orientation Dependence

In the original paper by Kuwata *et al.* [5], which reported the superiority of 0.91PZN-0.09PT (electromechanical coupling factor $k_{33}^* = 95\%$ and the piezoelectric constant

$d_{33}{}^{*} = 1600$ pC/N), when the poling direction was 57° canted from the spontaneous polarization (P_S) direction [see Fig. 15(a)], they indicated the importance of the shear deformation mode. The piezoelectric constants $d_{[001]//}$ and $d_{[111]//}$ in the rhombohedral phase can be represented by using the fundamental piezoelectric components d_{31}, d_{33}, d_{22}, and d_{15} in 3m symmetry

$$d_{[001]//} = \left(2\sqrt{2}\, d_{22} + 2d_{31} + d_{33} + 2d_{15}\right)/3\sqrt{3} \quad (72a)$$

$$d_{[111]//} = d_{33}. \quad (72b)$$

The shear-mode component d_{15} is larger than d_{33} and d_{22} in many perovskite FEs, which plays an important role in the formulas. The ratio $d_{[001]//}/d_{[111]//}$ of 0.91PZN-0.09PT is 2.5 in the rhombohedral phase; significant enhancement in the effective d_{33}^{*} $(= d_{[001]//})$ is anticipated by canting the electric field direction 57°.

This original idea has been expanded later to "rotator and extender FEs" by Davis *et al.* [83]. Depending on the value of d_{15} higher or lower in comparison with d_{33}, they are denoted "rotator" or "extender FEs," which are basically categorized as rhombohedral and tetragonal symmetry by collecting numerous data. In particular, PZN-0.07PT and PMN-0.33PT with rhombohedral (3m) symmetry exhibit significantly large $d_{[001]//}/d_{[111]//}$ values, 65 and 22, respectively, which are compared with 3.4 of rhombohedral PZ-0.40PT. On the contrary, some extreme tetragonal (4 mm) compositions PMN-0.42PT and PZ-0.90PT give the ratios of 0.5 and 0.6, respectively, which means that no enhancement of piezoelectricity is expected by canting the electric field direction. The "rhombohedral" symmetry seems to be essential for obtaining the significant $d_{33}{}^{*}$ enhancement in practice.

The existence of the monoclinic phase in the "MPB" in PZN-PT and PMN-PT systems is argued in contrast to a model of the rhombohedral and tetragonal coexistence. Though the macroscopic phenomena may be similar experimentally, microscopic clarification and its theoretical explanation are required. These classic approaches are not related to the domain generation, but viable under a monodomain uniform state.

A relating topic with the crystal orientation in single crystals includes the electric-field-induced phase transition. Fig. 16 shows the longitudinal strain in PZN-4.5%PT and PZN-8%PT induced by the electric field along the ⟨001⟩ axis, reported by Park and Shrout [9]. The extra steep strain changes (shown by arrows) by 0.2%–0.3% seem to be associated with the rhombohedral-to-tetragonal phase transition under a high field. The slope of the strain curve around $E = 0$ corresponds approximately to the piezoelectric d constant. The domain configuration change in a [111] plate PZN-9%PT (i.e., MPB composition) with the phase transition is also inserted on the right-hand side [84]. This MPB composition crystal at zero electric fields seems to be composed of a tetragonal/rhombohedral lamellar structure (i.e., two-phase coexistence). The rhombohedral phase is characterized by the spindle-like domain pattern. Under a high electric field, the spindle-like domains disappear to become tetragonal domains

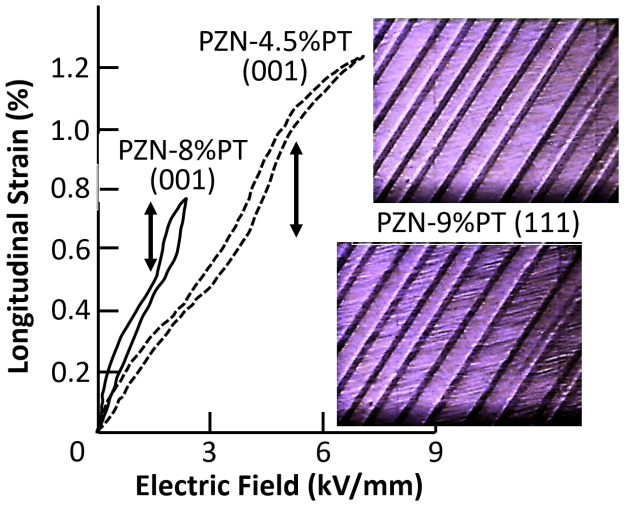

Fig. 16. Longitudinal strains induced in PZN-PT single crystals associated with the Rhomb.-to-Tet. phase transition. The domain configuration change with the phase transition is also inserted.

[see Fig. 16 (top)]. The substructure in the thick domain walls has not yet been clarified.

B. Domain Size Effect on the Piezoelectric Performance

With increasing the single-crystal PMN-PT applications for medical ultrasonic probe applications, we recognized that the canted *3m* monodomain crystal exhibits unnecessary shear vibration modes under a plate excitation along the perovskite ⟨100⟩ axis. In order to handle this crystal plate as the pure k_{33}-like mode, the macroscopic crystal symmetry should be modified to *4mm*. From this motivation, the single-crystal manufacturers tried to make a crystal with as close a volumetric ratio as possible to the four equivalent polarization domains, as illustrated in Fig. 15(b), which may be the initial phase of the domain engineering. That is, uniform volumetric distribution of the four polarization domains is required in a finite ultrasonic probe element (typically sub-mm size)

In order to achieve giant "electrostriction" in relaxor FEs, such as 0.9PMN-0.1PT, or piezostriction in 0.72PMN–0.28PT, a uniform microdomain is preferred to reduce the strain hysteresis under an electric field applied by sacrificing the strain magnitude. Thus, the grain size was carefully controlled in practical actuator materials [85]. Knowing the fact that the domain size is proportional to the grain size, and the electric-field-induced strain is increased with the grain size, we can anticipate the piezoelectric performance (real part such as piezoelectric d constant) to increase with the domain size increase, in general.

On the other hand, some researchers are reporting the opposite results and computer simulations. Cao's group reported piezoelectric properties for $[001]_c$ poled $0.94Pb(Zn_{1/3}Nb_{2/3})O_3$-$0.06PbTiO_3$ single crystals by changing the domain size from 20 down to 8 μm [see Fig. 17(a)] [86]. They clearly demonstrated the piezoelectric $d_{33}{}^{*}$ monotonous increase from 2200 to 3400 pC/N according to the domain size reduction. Morozovska *et al.* [87] proposed computer simulation models on the effective piezoelectric

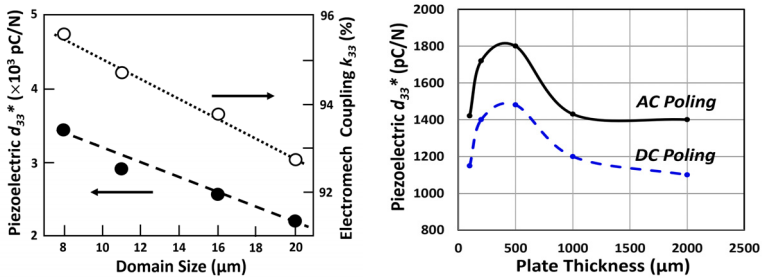

Fig. 17. (a) Measured piezoelectric properties in different domain sizes [001]-poled PZN-6%PT single crystals [86]. (b) Comparisons of effective piezoelectric coefficients for the dc- and ac-poled samples with different thicknesses [91].

response from the twin walls in FEs using $BaTiO_3$ for example. Their twin-domain boundary model suggested a significant enhancement in polarization and associated shear mode d piezoelectric coupling around ± 10 nm of the twin boundary, as illustrated in Fig. 15(c). Thus, they proposed that a smaller domain configuration is preferable to the d enhancement.

C. Domain Engineering

The most recent trend seems to return to "the larger the domain is, the better the performance is." Many researchers use the ac poling (ACP) process (invented by Yamamoto *et al.* [88]) to enhance piezoelectric properties for PMN-PT in comparison with conventional dc poling (DCP) [89]–[91]. For perovskite [001]-oriented rhombohedral PMN–0.28PT single crystals, Qiu *et al.* [91] claimed that increasing the thickness of the perovskite (001) plate specimen led to a higher d_{33} value from 100, 200, and 500 μm [see Fig. 17(b)], in which we may expect an increase in the domain size; thus, it seems to be contradictory to the papers introduced in the previous subsection (i.e., (normal to the general sense). The degradation of the $d_{33}{}^*$ value for 1 and 2 mm is not clear but may be related to a sort of "clamping." They reported more than 20% higher $d_{33}{}^*$ improvement under the ACP over the DCP specimens. Though the ACP process has various advantages, the ACP process also reveals a large standard deviation of $\varepsilon_{33}^X/\varepsilon_0$ value compared with that of DCP according to the poling conditions. The large standard deviation of permittivity makes it difficult to design a high-quality medical array probe for mass production. Yamashita's group demonstrated a high piezoelectric coefficient $d_{33} > 1950$ pC/N in PMN–0.28PT single crystals obtained by low-voltage ACP of 1.5–3.5 kV_{RMS}/cm at a high temperature of 80 °C in an air atmosphere (different from the conventional silicone oil immersion) [89]. The minimum standard deviation of 170 was similar to conventional DCP and a high average $\varepsilon_{33}^X/\varepsilon_0$ of 8800 was confirmed with a 2.0 kV_{RMS}/cm of ACP for five specimens.

The ac electric field has an ability to efficiently merge the FE domains on both sides of 71° domain walls, leading to a considerable increase in the domain size and, thus, a significant enhancement of electromechanical properties, as illustrated in Fig. 15(d). Qiu *et al.* [91] also demonstrated a computer simulation for the domain size increase to create lamellar configurations during the ACP process. Fig. 15(d) indicates that, for the ac-poled $[001]_C$-oriented rhombohedral PMN-PT crystal, the most stable state should be the lamellar domain structure (almost uniform periodic distance) with only 109° domain walls and the same volume fractions of the two types of FE domains on both sides of domain walls, just by eliminating the vertical domain walls. This domain configuration is expected to benefit the design of high-performance FE via domain or domain wall engineering. A problem in this simulation is the 2-D plate lamellar structure, the fractal dimension of which should be 1. Because 1-D spindle-like domain patterns are typically observed in relaxor FEs, an advanced simulation is desired in order to satisfy the fractal dimension $D = 2$. This ACP process also reflects the coercive field reduction and piezoelectric d_{33}^* enhancement. Though the dielectric loss does not increase through the ACP process, the author is anticipating the mechanical quality factor (i.e., elastic loss) degradation with the vibration velocity for this "softening" process, which blocks high-power piezoelectric applications. Immediate clarification on this possible problem is desired.

X. Conclusion: Key Points and Future Perspectives

As mentioned in Section IX, recent studies on PMN-PT single crystals seem to be focusing more on domain engineering in order to improve the electromechanical coupling performances for practical applications. We do rarely find papers that try to answer directly why PMN or PZN reveals an enormous piezoelectric effect beyond Kuwata *et al.*'s original idea on the crystal orientation dependence (that is, the shear k_{15} contribution). The induced "monoclinic phase" model is still a similar modification to the above "shear" model. After the historical discovery background, this article described key factors for understanding why the relaxor/complex perovskites exhibit superior electromechanical/electrostrictive coupling and for developing new materials for actuators and transducers from the author's personal strategies. These factors include: 1) interrelation between complex perovskite structure and ferroelectricity; 2) anharmonicity in relaxor FEs; and 3) microdomain contribution in relaxor FEs.

In this section, the author will describe the research directions for future successors in this field.

1) *Electrostriction Phenomenology of Antiferroelectrics:* It is noteworthy that intersublattice couplings q_{33} and

q_{31} have the same positive sign, while intrasublattice couplings Q_{33} and Q_{31} have the opposite sign showing a normal "piezoelectric Poisson's ratio" of ∼1/3. The theoretical explanation on the "negative Poisson's ratio" (i.e., isotropic volumetric expansion) among the intersublattice couplings q_{33} and q_{31} is a future problem to be explained. This is important to develop high piezoelectric anisotropy (i.e., $|d_{33}/d_{31}|$) materials for medical diagnostic acoustic probes.

2) *Complex Perovskite Ion Ordering Versus Ferroelectric Properties:* Disorder and 1:1 ordered complex perovskites tend to reveal FE and AFE properties, respectively. The electrostrictive coefficient Q increases with cation order from disordered, through partially ordered, simple, and then ordered perovskites, while the effective Curie–Weiss constant C (determined from the average slope of $1/\varepsilon$ just above the T_C) decreases in this sequence, leading to the product of Q and C^{eff} nearly constant for all FE and AFE perovskites [$Q_h C = 3.1(\pm 0.4) \times 10^3 \text{m}^4\text{C}^{-2}\text{K}$]. Though the "rattling ion model" explains intuitively these rules, a more detailed theoretical discussion should be made in the future.
3) Disorder with some short-range order tendency in PMN-PT seems to be the primary key in practice to create giant electrostriction and an enormous electromechanical coupling factor. The ion ordering principle was discussed by Patrat *et al.* [27] on $Sr(Fe^{3+}_{1/2}Ta^{5+}_{1/2})O_3$. The ordered structure is preferable from the Madelung energy viewpoint, while the polarization energy stabilizes the disordered structure. "Displacement energy" originated from the ionic radius difference among Fe^{3+} and Ta^{5+} stabilizes the disorder structure because its contribution is small due to similar ionic radii among these ions. If the ionic radii of two B ions differ significantly, the order structure will become stable. It would be interesting to study ordered and disordered crystals with the same composition, in which the degree of order is controlled by annealing, such as $Pb(Sc_{1/2}Ta_{1/2})O_3$ [28]. The advanced thermodynamical theory is expected to predict antiferroelectricity with the degree of ionic ordering.
4) *Anharmonicity of Lattice Vibration in Relaxor Ferroelectrics:* The soft phonon (TO) mode is expressed as $(\Omega^{\text{soft}}_{\text{TO}})^2 = A(T - T_C)$. In order to explain the smaller electrostrictive Q constant and larger Curie–Weiss constant C in relaxor FEs, in comparison with normal types, an order of magnitude lower A constant was verified by the recent advanced equipment [59], [61]. It would also be interesting to study the soft phonon frequency change with the degree of ionic order in crystals, in which the order is controllable by annealing. One remaining problem is Samara's empirical rule: the $(\partial(T_C)/\partial p)$ value is roughly constant for all perovskite FEs, which waits for detailed theoretical approaches.
5) *Critical Exponent of Permittivity in Relaxor Ferroelectrics:* The critical exponent γ in the temperature dependence of permittivity in a generalized form: $(1/\varepsilon - 1/\varepsilon_m) = C'^{-1}(T - T_m)^{\gamma}$, not only for relaxor FEs but also for normal sharp-transition FEs. This exponent fitting agrees very well in a wide temperature range. Sharp phase transition BT has a γ value nearly equal to 1: this corresponds to the Curie–Weiss law. The solid solution KTN with an "apparent" sharp transition with a slight deviation from the Curie–Weiss law gives $\gamma = 1.17$. On the other hand, the γ value is as large as 1.7 for PMN and PZN with a very diffused transition, however, relatively smaller than expected "2" for the "quadratic law." The "critical exponent" in relaxor FEs indicated the microdomain–microdomain interaction explicitly, different from the statistical isotropic models, such as the Gaussian model or the Vogel–Fulcher model.
6) *Fractal Analysis of Microdomain Configuration:* The "scaling function" $g(\lambda)$ has a general formula: $g(\lambda) = \lambda^p$, where p can be noninteger. We can translate this function in relaxor FEs as follows: the PNR corresponds to "cluster," which has the Curie temperature T_C distribution $(T_C - T_{\text{av}})$ due to the composition (or position) fluctuation $(x - x_{\text{av}})$. Taking $(T - T_{\text{av}})$ as a scaling parameter λ, based on the local Curie–Weiss law $(1/\varepsilon - 1/\varepsilon_m) \propto (T - T_m)$ in each microcluster, the "scaling function" corresponds to the inverse permittivity; then, the following critical exponent equation is expected $(1/\varepsilon - 1/\varepsilon_{\max}) \propto (T - T_{\text{av}})^p$. Aburatani *et al.* proposed the AE measurement for determining the "fractal dimension" D. D of the normal FE PZT ceramics in the electric-field-induced strain consisted of the domain reorientation related $D = 1$ and the domain reorientation-unrelated $D = 2.8$ when a high electric field cycle is applied. $D = 2$ is obtained in the electrostrictive PMN-PT (i.e., relaxor). An intuitive domain dynamic model was proposed: clear plate-like 90° domain walls move primarily perpendicular to the plate (1-D motion) in normal FEs (e.g., PZT). However, when the electric field is much larger than the coercive field in PZT, a monodomain-like state will be realized. The deformation beyond this field level is caused by intrinsic piezoelectricity (elastic deformation), that is, 3-D deformation, which suggests the fractal dimension $D = 2.8$. On the contrary, in PMN-PT, spindle-like microdomains breathe by keeping the length, which indicates that $D = 2$ from this microdomain dynamics. The fractal dimension determination may suggest the microdomain growth mechanisms, which will enhance the "domain engineering" insight. This point is the key difference from the conventional statistical isotropic models, such as the Gaussian model or the Vogel–Fulcher model. Expanding the fractal analysis, clarification of the relationship between the critical exponent γ and the fractal dimension D is a remaining research topic.
7) *Domain Engineering:* Is "the larger the domain size is, the better the piezoelectric performance is" true? How can we explain the contradictory empirical results reported by Cao's group in Fig. 17(a)? Solving this "dilemma" is an immediate research topic. Because the relaxor single crystals reveal microdomain spontaneously, enhanced "electrostriction" performance seems

to be anticipated in "finer" microdomain specimen in the "apparently" paraelectric phase. The domain twin-boundary in the FE state seems to enhance the piezoelectric performance, which suggests the preference for the fine domain configuration. Recent "ac electric-poling" can generate uniform lamellar semi-macrodomains, which enhances the piezoelectric $d_{33}{}^*$ by 20%. We need to investigate deeper to see which model will be more suitable among "twin-domain-boundary" and "ACP domain growth" or to see how we should compromise these ideas in order to solve the above "dilemma." Through the ACP process can enhance the $d_{33}{}^*$ and k_{33}, the author is anticipating the mechanical quality factor (i.e., elastic loss) degradation with the vibration velocity for this "softening" process, which may block this material from high-power piezoelectric applications. The high-power characterization should immediately be conducted.

8) Expanding the conventional statistical isotropic models, such as the Gaussian model or the Vogel–Fulcher model, the author desires to recruit the successors on the "fractal analysis" on the microdomain interaction, a bit different mesoscopic approach to distinguish the electromechanical coupling among the normal and relaxor FEs.

REFERENCES

[1] L. E. Cross, S. J. Jang, R. E. Newnham, S. Nomura, and K. Uchino, "Large electrostrictive effects in relaxor ferroelectrics," *Ferroelectrics*, vol. 23, no. 1, pp. 187–191, Jan. 1980.

[2] K. Uchino, S. Nomura, L. E. Cross, S. J. Jang, and R. E. Newnham, "Electrostrictive effect in lead magnesium niobate single crystals," *J. Appl. Phys.*, vol. 51, no. 2, pp. 1142–1145, Feb. 1980.

[3] K. Uchino, S. Nomura, L. E. Cross, R. E. Newnham, and S. J. Jang, "Electrostrictive effect in perovskites and its transducer applications," *J. Mater. Sci.*, vol. 16, no. 3, pp. 569–578, Mar. 1981.

[4] J. Kuwata, K. Uchino, and S. Nomura, "Phase transitions in the Pb $(Zn_{1/3}Nb_{2/3})O_3$-$PbTiO_3$ system," *Ferroelectrics*, vol. 37, no. 1, pp. 579–582, 1981.

[5] J. Kuwata, K. Uchino, and S. Nomura, "Dielectric and piezoelectric properties of $0.91Pb(Zn_{1/3}Nb_{2/3})O_3$-$0.09PbTiO_3$ single crystals," *Jpn. J. Appl. Phys.*, vol. 21, no. 9, pp. 1298–1302, 1982.

[6] T. Sato, H. Ishikawa, O. Ikeda, K. Uchino, and S. Nomura, "Multilayer PMN coherent optical adaptive technique," *J. Opt. Soc. Amer.*, vol. 71, no. 12, p. 1645, 1981.

[7] B. Wada, *Hubble Telescope Structure*, JPL document D-10659, 1993, p. 23.

[8] K. Yanagisawa, H. Kanai, and Y. Yamashita, "Hydrothermal crystal growth of lanthanum-modified lead zirconate titanate" *Japan. J. Appl. Phys.*, vol. 34, no. 9B, p. 536, 1995.

[9] S.-E. Park and T. R. Shrout, "Ultrahigh strain and piezoelectric behavior in relaxor based ferroelectric single crystals," *J. Appl. Phys.*, vol. 82, no. 4, pp. 1804–1811, Aug. 1997.

[10] A. F. Devonshire, "Theory of ferroelectrics," *Adv. Phys.*, vol. 3, no. 10, pp. 85–130, 1954.

[11] H. F. Kay, "Electrostriction," *Rep. Prog. Phys.*, vol. 18, no. 1, p. 230, 1955.

[12] G. A. Samara, "The effects of hydrostatic pressure on ferroelectric properties," *J. Phys. Cos. Jpn.*, vol. 285, p. 399, Mar. 1970.

[13] K. Uchino, "Electrostrictive bimorph force sensors," in *Proc. Study Committee Barium Titanate XXXI*, 1983, pp. -171–1067.

[14] C. Kittel, "Theory of antiferroelectric crystals," *Phys. Rev.*, vol. 82, no. 5, pp. 729–732, Jun. 1951.

[15] S. Fujimoto and N. Yasuda, "Phenomenological treatment of antiferroelectric transition under hydrostatic pressure," *Jpn. J. Appl. Phys.*, vol. 15, no. 4, pp. 595–600, Apr. 1976.

[16] K. Uchino, "Electrostrictive Effect in Antiferroelectrics," *Solid State Phys.*, vol. 17, p. 371, Mar. 1982.

[17] K. Uchino, L. E. Cross, R. E. Newnham, and S. Nomura, "Electrostrictive effects in antiferroelectric perovskites," *J. Appl. Phys.*, vol. 52, no. 3, pp. 1455–1459, Mar. 1981.

[18] K. Uchino and S. Nomura, "Electrostriction in PZT-family antiferroelectrics," *Ferroelectrics*, vol. 50, no. 1, pp. 191–196, Nov. 1983.

[19] K. Uchino, "Digital displacement transducer using antiferroelectrics," *Jpn. J. Appl. Phys.*, vol. 24, no. S2, p. 460, Jan. 1985.

[20] K.-Y. Oh, Y. Saito, A. Furuta, and K. Uchino, "Piezoelectricity in the field-induced ferroelectric phase of lead zirconate-based antiferroelectrics," *J. Amer. Ceram. Soc.*, vol. 75, no. 4, pp. 795–799, Apr. 1992.

[21] K. Uchino and K. Y. Oh, "Piezoelectric anisotropy and polarization sublattice coupling in perovskite crystals," *J. Amer. Ceram. Soc.*, vol. 74, no. 5, pp. 1131–1134, 1991.

[22] H. Takeuchi, S. Jyomura, E. Yamamoto, and Y. Ito, "Electromechanical properties of (Pb, Ln) (Ti, Mn) O_3 ceramics (Ln = rare earths)," *J. Acoust. Soc. Amer.*, vol. 72, no. 4, p. 1114, 1982.

[23] Y. Yamashita, K. Yokoyama, H. Honda, and T. Takahashi, "(Pb, Ca) $((Co_{1/2}W_{1/2}), Ti)O_3$ piezoelectric ceramics and their applications," *Jpn. J. Appl. Phys.*, vol. 20, no. S4, p. 183, 1981.

[24] W. Kinase, Y. Uemura, and M. Kikuchi, "Correction of dipole field due to lattice deformation of a perovskite-type crystal," *J. Phys. Chem. Solids*, vol. 30, pp. 441–447, Feb. 1969.

[25] R. S. Roth, "Classification of perovskite and other ABO3-type compounds," *J. Res. Nat. Bur. Standards*, vol. 58, p. 75, Apr. 1957.

[26] G. Blasse and A. F. Corsmit, "Electronic and vibrational spectra of ordered perovskites," *J. Solid State Chem.*, vol. 6, pp. 513–518, Apr. 1973.

[27] G. Patrat, M. Brunel, and F. de Bergevin, "Ordre a courte distance et energie interne des composes Sr_2TaFeO_6 et Sr_2TaCrO_6 de type perovskite," *J. Phys. Chem. Solids*, vol. 37, no. 3, pp. 285–291, Jan. 1976.

[28] N. Setter and L. E. Cross, "The role of B-site cation disorder in diffuse phase transition behavior of perovskite ferroelectrics," *J. Appl. Phys.*, vol. 51, p. 4356, Jul. 1980.

[29] S. Nomura, K. Toyama, and K. Kaneta, "$Ba(Mg_{1/3}Ta_{2/3})O_3$ ceramics with temperature-stable high dielectric constant and low microwave loss," *Jpn. J. Appl. Phys.*, vol. 21, no. 10A, p. L624, 1982.

[30] K. Uchino, L. E. Cross, R. E. Newnham, and S. Nomura, "Electrostrictive effects in non-polar perovskites," *Phase Transitions*, vol. 1, no. 4, pp. 333–341, Nov. 1980.

[31] A. Amin, R. E. Newnham, L. E. Cross, S. Nomura, and D. E. Cox, "Ordering in Pb $(Mg_{13}Nb_{23})O_3$-$Pb(Mg_{12}W_{12})O_3$ solid solutions," *J. Solid State Chem.*, vol. 35, pp. 267–271, Nov. 1980.

[32] Y. M. Poplavko, *Sov. Phys. Solid State*, vol. 27, p. 1903, 1985.

[33] D. Viehland, S. J. Jang, L. E. Cross, and M. Wuttig, "Deviation from curie-weiss behavior in relaxor ferroelectrics," *Phys. Rev. B, Condens. Matter*, vol. 46, no. 13, pp. 8003–8006, Oct. 1992.

[34] J. Toulouse, "The three characteristic temperatures of relaxor dynamics and their meaning," *Ferroelectrics*, vol. 369, no. 1, pp. 203–213, Oct. 2008.

[35] C. G. F. Stenger and A. J. Burggraaf, "Order–disorder reactions in the ferroelectric perovskites $Pb(Sc_{1/2}Nb_{1/2})O_3$ and $Pb(Sc_{1/2}Ta_{1/2})O_3$. II. Relation between ordering and properties," *Phys. Status Solidi (A)*, vol. 61, pp. 653–664, Oct. 1980.

[36] C. Lei, A. A. Bokov, and Z.-G. Ye, "Ferroelectric to relaxor crossover and dielectric phase diagram in the $BaTiO_3$–$BaSnO_3$ system," *J. Appl. Phys.*, vol. 101, no. 8, 2007, Art. no. 084105.

[37] F. Li, L. Jin, Z. Xu, and S. Zhang, "Electrostrictive effect in ferroelectrics: An alternative approach to improve piezoelectricity," *Appl. Phys. Rev.*, vol. 1, no. 1, Mar. 2014, Art. no. 011103, doi: 10.1063/1.4861260.

[38] K. Uchino, *Ferroelectric Devices*, 2nd ed. New York, NY, USA: CRC Press, 2010.

[39] M. Born and M. Göppert-Mayer, *Handbuch der Physik*, vol. 24. Berlin, Germany: Springer, 1933, p. 623.

[40] K. Uchino and L. E. Cross, "Electrostriction and its interrelation with other anharmonic properties of materials," *Jpn. J. Appl. Phys.*, vol. 19, no. 4, pp. L171–L173, Apr. 1980.

[41] N. W. Ashcroft and N. D. Mermin, *Solid State Physics*. Orlando, FL, USA: W. B. Saunders, 1976.

[42] C. Kittel, *Solid State Physics*, 5th ed. New York, NY, USA: Wiley, 1976.

[43] J. Kuwata, K. Uchino, and S. Nomura, "Electrostrictive coefficients of $Pb(Mg_{1/3}Nb_{2/3})O_3$ ceramics," *Jpn. J. of Appl. Phys.*, vol. 19, no. 11, pp. 2099–2103, 1980.

[44] K. Uchino, S. Nomura, and L. E. Cross, "Anomalous temperature dependence of electrostrictive coefficients in $K(Ta_{0.55}Nb_{0.45})O_3$," *J. Phys. Soc. Jpn.*, vol. 51, no. 10, pp. 3242–3244, Oct. 1982.

[45] H. Uwe and T. Sakudo, "Electrostriction and stress-induced ferroelectricity in KTaO3," *J. Phys. Soc. Jpn.*, vol. 38, no. 1, pp. 183–189, Jan. 1975.
[46] E. Wiesendanger, "Dielectric, mechanical and optical properties of orthorhombic $KNbO_3$," *Ferroelectrics*, vol. 6, no. 1, p. 263, 1974.
[47] W. Cochran, "Crystal stability and the theory of ferroelectricity," *Adv. Phys.*, vol. 9, no. 36, pp. 387–423, 1960.
[48] T. Kurosawa, "Polarization waves in solids," *J. Phys. Soc. Jpn.*, vol. 16, no. 7, pp. 1298–1308, 1961.
[49] R. H. Lyddane, R. G. Sacks, and E. Teller, "On the polar vibrations of alkali halides," *Phys. Rev.*, vol. 59, p. 673, Apr. 1941.
[50] K. Ishii, "Vibration and eigenvalue problem," *Mod. Math.*, vol. 5, no. 1, pp. 24–32, 1972.
[51] P. Pichanusakorn and P. Bandaru, "Nanostructured thermoelectrics," *Mater. Sci. Eng., R, Rep.*, vol. 67, nos. 2–4, pp. 19–63, Jan. 2010, doi: 10.1016/j.mser.2009.10.001.
[52] G. Burns and B. A. Scott, "Determination of stoichiometry variations in $LiNbO_3$ and $LiTaO_3$ by Raman powder spectroscopy," *J. Amer. Ceram. Soc.*, vol. 56, p. 225, May 1973.
[53] K. Uchino, S. Nomura, L. E. Cross, and R. E. Newnham, "Soft modes in relaxor ferroelectrics," *Phase Transitions*, vol. 2, no. 1, pp. 1–6, Jan. 1981.
[54] B. N. Rolov, *Fiz. Tverdogo Tel*, vol. 6, p. 2128, 1963.
[55] P. A. Fleury and J. M. Worlock, "Electric-field-induced Raman scattering in $SrTiO_3$ and $KTaO_3$," *Phys. Rev.*, vol. 174, p. 613, Oct. 1968.
[56] G. Shirane, J. D. Axe, J. Harada, and J. P. Remeika, "Soft ferroelectric modes in lead titanate," *Phys. Rev. B, Condens. Matter, Condens. Matter*, vol. 2, no. 1, pp. 155–159, Jul. 1970.
[57] A. Al-Zein, J. Hlinka, J. Rouquette, and B. Hehlen, "Soft mode doublet in $PbMg_{1/3}Nb_{2/3}O_3$ relaxor investigated with hyper-Raman scattering," *Phys. Rev. Lett.*, vol. 105, Jun. 2010, Art. no. 017601.
[58] H. Taniguchi, M. Itoh, and D. Fu, "Raman scattering study of the soft mode in $Pb(Mg_{1/3}Nb_{2/3})O_3$," *J. Raman Spectrosc.*, vol. 42, pp. 706–714, Apr. 2011.
[59] B. Hehlen, M. Al-Sabbagh, A. Al-Zein, and J. Hlinka, "Relaxor ferroelectrics: Back to the single-soft-mode picture," *Phys. Rev. Lett.*, vol. 117, no. 15, Oct. 2016, Art. no. 155501.
[60] D. H. Kim, J.-H. Ko, C. D. Feng, and S. Kojima, "Micro-Brillouin scattering study of ferroelectric relaxor $Pb[(Zn_{1/3}Nb_{2/3})_{0.91}Ti_{0.09}]O_3$ single crystals under the electric field along the [001] direction," *J. Appl. Phys.*, vol. 98, Mar. 2005, Art. no. 044106.
[61] S. Kojima and J.-H. Ko, "Broadband micro-Brillouin scattering spectroscopy of $Pb(B_{1/3}B'_{2/3})O_3$-based relaxor ferroelectrics," *Current Appl. Phys.*, vol. 11, pp. S22–S32, May 2011, doi: 10.1016/j.cap.2011.04.038.
[62] G. A. Smonlensky, V. A. Isupov, A. I. Agranovskaya, and S. N. Popov, "Ferroelectrics with diffuse phase transitions," *Sov. Phys.-Solid State*, vol. 2, no. 1, pp. 2584–2594, 1961.
[63] S. Nomura and F. Kojima, "Dielectric relaxation and thermal stimulated current in $(K_{3/4}Bi_{1/4})(Zn_{1/6}Nb_{5/6})O_3$ and its solid solutions," *Jpn. J. Appl. Phys.*, vol. 12, no. 2, p. 205, 1973.
[64] G. I. Skanavi, I. M. Ksendzov, V. A. Trigubenko, and V. G. Prokhvatilov, "Relaxation polarization and losses in nonferroelectric dielectrics with high dielectric constants," *Sov. Phys. JETP*, vol. 6, pp. 250–259, Feb. 1958.
[65] D. Viehland, J. F. Li, S. J. Jang, L. E. Cross, and M. Wuttig, "Glassy polarization behavior of relaxor ferroelectrics," *Phys. Rev. B, Condens. Matter*, vol. 46, no. 13, pp. 8013–8017, Oct. 1992.
[66] V. A. Isupov, *Zh. Tech. Fiz.*, vol. 26, p. 1912, 1956.
[67] V. A. Isupov, *Izv. Akad. Nauk SSSR, Ser. Fiz.*, vol. 28, p. 653, 1964.
[68] J. Kuwata, K. Uchino, and S. Nomura, "Diffuse phase transition in lead zinc niobate," *Ferroelectrics*, vol. 22, no. 1, pp. 863–867, 1979.
[69] K. Uchino, J. Kuwata, S. Nomura, L. E. Cross, and R. E. Newnham, "Interrelation of electrostriction with phase transition diffuseness–improvement of the temperature characteristics of electrostriction," *Jpn. J. Appl. Phys.*, vol. 20, no. 4, p. 171, 1981.
[70] W. Känzig, *Helv. Phys. Acta*, vol. 24, p. 175, 1951.
[71] H. B. Krause, J. M. Cowley, and J. Wheatley, "Short-range ordering in $PbMg_{1/3}Nb_{2/3}O_3$," *Acta Crystallographica A*, vol. A35, no. 6, pp. 1015–1017, 1979.
[72] K. Uchino and S. Nomura, "Critical exponents of the dielectric constants in diffused-phase-transition crystals," *Ferroelectrics*, vol. 44, no. 1, pp. 55–61, Apr. 1982.
[73] L. E. Cross, "Relaxorferroelectrics: An overview," *Ferroelectrics*, vol. 151, no. 1, pp. 305–320, 1994.
[74] G. A. Samara, "Pressure and temperature dependences of the dielectric properties of the perovskites $BaTiO_3$ and $SrTiO_3$," *Phys. Rev.*, vol. 151, p. 378, Nov. 1966.
[75] G. A. Smolenskii, *J. Phys. Soc. Jpn.*, vol. 28, p. 26, 1970.
[76] M. L. Mulvihill, L. E. Cross, and K. Uchino, "Dynamic motion of the domain configuration in relaxor ferroelectric single crystals as a function of temperature and electric field," in *Proc. 8th Eur. Mtg. Ferroelectr., Ferroelectr.*, vol. 186, 1996, pp. 325–328.
[77] H. Aburatani, J. P. Witham, and K. Uchino, "A fractal analysis on domain related electric field induced acoustic emission in ferroelectric ceramics," *Jpn. J. Appl. Phys.*, vol. 37, no. 2R, pp. 602–605, 1998.
[78] K. Uchino, "Fractal phenomena in ferroelectrics," *J. Nanotech. Mater. Sci.*, vol. 1, no. 1, pp. 1–15, 2014.
[79] H. Nakasa, *Theoretical Bases and Applications of Acoustic Emission*, 1st, ed. Tokyo, Japan: Chijin Shokan, 1994.
[80] V. Y. Shur *et al.*, "Fractal clusters in relaxor PLZT ceramics: Evolution in electric field," *Ferroelectrics*, vol. 299, no. 1, pp. 75–81, Jan. 2004.
[81] A. Koreeda, "Fractal dynamics in relaxor ferroelectrics," *Bull. Jpn. Ceram. Soc.*, vol. 48, no. 7, pp. 537–541, 2013.
[82] H. E. Stanley, *Introduction to Phase Transitions and Critical Phenomena*. Oxford, U.K.: Clarendon Press, 1971, ch. 8.
[83] M. Davis, M. Budimir, D. Damjanovic, and N. Setter, "Rotator and extender ferroelectrics: Importance of the shear coefficient to the piezoelectric properties of domain-engineered crystals and ceramics," *J. Appl. Phys.*, vol. 101, no. 5, Mar. 2007, Art. no. 054112, doi: 10.1063/1.2653925.
[84] R. Ujiie and K. Uchino, "Dynamical domain observation in relaxor ferroelectrics," in *Proc. IEEE Symp. Ultrason.*, Dec. 1990, pp. 725–728.
[85] K. Uchino, M. Tatsumi, I. Hayashi, and T. Hayashi, "Grain size dependence of electrostriction in PMN ceramics," *Jpn. J. Appl. Phys.*, vol. 24, no. S2, pp. 733–735, 1985.
[86] Y. Xiang, R. Zhang, and W. Cao, "Optimization of piezoelectric properties for $[001]_c$ poled $0.94Pb(Zn_{1/3}Nb_{2/3})O_3$–$0.06PbTiO_3$ single crystals," *Appl. Phys. Lett.*, vol. 96, no. 9, 2010, Art. no. 092902.
[87] A. N. Morozovska, E. A. Eliseev, O. V. Varenyk, and S. V. Kalinin, "Effective piezoelectric response of twin walls in ferroelectrics," *J. Appl. Phys.*, vol. 113, no. 18, May 2013, Art. no. 187222, doi: 10.1063/1.4801988.
[88] N. Yamamoto, Y. Yamashita, Y. Hosono, K. Itsumi, and K. Higuchi, "Method of manufacturing ultrasonic probe and method of manufacturing piezoelectric transducer," U.S. Patent 0062261 A1, 2014.
[89] Y. Sun, T. Karaki, T. Fujii, and Y. Yamashita, "Enhanced electric property of relaxor ferroelectric crystals with low AC voltage high-temperature poling," *Jpn. J. Appl. Phys.*, vol. 59, no. SP, Nov. 2020, Art. no. SPPD08, doi: 10.35848/1347-4065/abb2ff.
[90] C. Qiu, J. Liu, F. Li, and Z. Xu, "Thickness dependence of dielectric and piezoelectric properties for alternating current electric-field-poled relaxor-$PbTiO_3$ crystals," *J. Appl. Phys.*, vol. 125, no. 1, Jan. 2019, Art. no. 014102, doi: 10.1063/1.5063682.
[91] C. Qiu *et al.*, "Transparent ferroelectric crystals with ultrahigh piezoelectricity," *Nature*, vol. 577, no. 7790, pp. 350–354, Jan. 2020.
[92] K. Uchino, *Micromechatronics*, 2nd ed. Boca Raton, FL, USA: CRC Press, 2020.

Kenji Uchino (Life Fellow, IEEE) received the Ph.D. degree from the Tokyo Institute of Technology, Tokyo, Japan, in 1981.

He was the Founder and a Senior Vice-President of Micromechatronics Inc., State College, PA, USA, from 2004 to 2010, where he was the Associate Director of the Office of Naval Research—Global from 2010 to 2014. He became a Research Associate at the Tokyo Institute of Technology in 1976. He joined Sophia University, Tokyo, as Associate Professor, in 1985. He was recruited from The Penn State University, State College, in 1991, as a Professor and the Director of the International Center for Actuators & Transducers. He is currently a Pioneer in piezoelectric actuators and a Professor Emeritus with The Penn State University. He has authored 582 papers, 84 books, and 33 patents in the ceramic actuator area.

Dr. Uchino is also a Fellow Life Member of the American Ceramic Society and a Senior Member of the National Academy of Inventors. He was a recipient of 31 awards, including the Distinguished Lecturer of the IEEE UFFC Society in 2018, the International Ceramic Award from the Global Academy of Ceramics in 2016, the IEEE-UFFC Ferroelectrics Recognition Award in 2013, the SPIE Smart Product Implementation Award in 2007, the R&D 100 Award in 2007, and the ASME Adaptive Structures Prize in 2005.